Title

Single-Cell Imaging of Metastatic Potential of Cancer Cells

Authors

Midde, Krishna
Sun, Nina
Rohena, Cristina
et al.

Publication Date

2018-12-01

DOI

10.1016/j.isci.2018.11.022

Peer reviewed

iScience

CellPress

Article

Single-Cell Imaging of Metastatic Potential of Cancer Cells

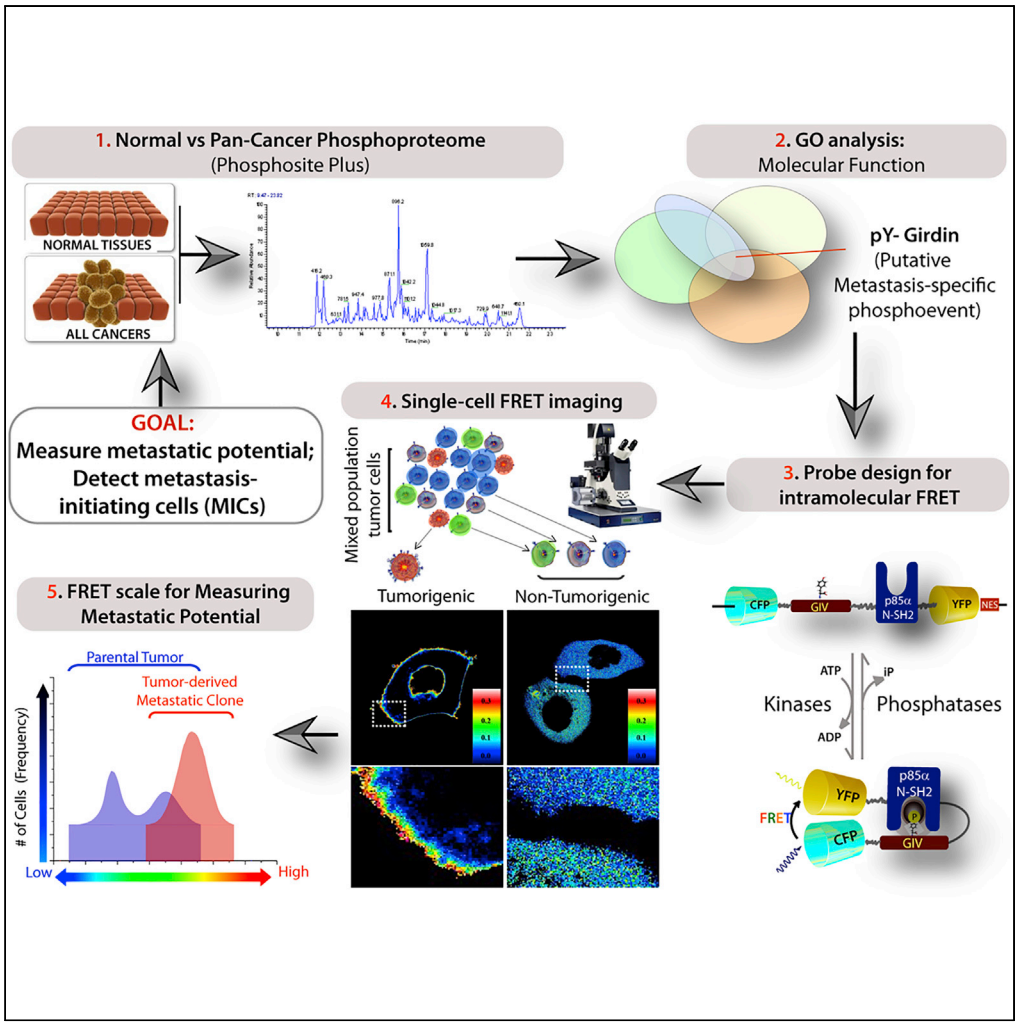

Krishna Midde, Nina Sun, Cristina Rohena, Linda Joosen, Harsharan Dhillon, Pradipta Ghosh

prghosh@ucsd.edu

HIGHLIGHTS

Phosphoproteomes of cancers predicted a putative metastasis-specific phosphoevent

FRET-based biosensor designed to assess this phosphoevent in living cells

Biosensor tracks the diversity and plasticity of metastatic potential of cancer cells

These sensors could direct drug efficacy testing against the most sinister cancer cells

Midde et al., iScience *10*, 53–65
December 21, 2018
https://doi.org/10.1016/j.isci.2018.11.022

iScience

CellPress

Article

Single-Cell Imaging of Metastatic Potential of Cancer Cells

Krishna Midde,[1,4] Nina Sun,[1,4] Cristina Rohena,[1] Linda Joosen,[1] Harsharan Dhillon,[1] and Pradipta Ghosh[1,2,3,5,*]

SUMMARY

Molecular imaging of metastatic "potential" is an unvanquished challenge. To engineer biosensors that can detect and measure the metastatic "potential" of single living cancer cells, we carried out a comprehensive analysis of the pan-cancer phosphoproteome to search for actin remodelers required for cell migration, which are enriched in cancers but excluded in normal cells. Only one phosphoprotein emerged, tyr-phosphorylated CCDC88A (GIV/Girdin), a bona fide metastasis-related protein across a variety of solid tumors. We designed multi-modular biosensors that are partly derived from GIV, and because GIV integrates prometastatic signaling by multiple oncogenic receptors, we named them "'integrators of metastatic potential (IMP)." IMPs captured the heterogeneity of metastatic potential within primary lung and breast tumors at steady state, detected those few cells that have acquired the highest metastatic potential, and tracked their enrichment during metastasis. These findings provide proof of concept that IMPs can measure the diversity and plasticity of metastatic potential of tumor cells in a sensitive and unbiased way.

INTRODUCTION

Metastasis is the dissemination of highly invasive cancer cells from the primary tumor to distant vital organs and the principal cause of cancer-related deaths (McAllister and Weinberg, 2014). However, not all tumors are metastatic, and determining the metastatic proclivity of single tumor cells remains a major challenge due to several reasons. First, and arguably the biggest, hurdle is tumor molecular heterogeneity because finding the few cells (0.02% [McAllister and Weinberg, 2014]) that have the potential to metastasize, interspersed within a mass of tumor cells that will not metastasize, requires precise tools that can pick up a few "signals" amid the thunderous "noise." Second, our understanding of what imparts metastatic potential remains incomplete despite increased comprehension of a more detailed signaling network with central control nodes (McAllister and Weinberg, 2014) and biomarkers that can detect such potential across different carcinomas are still lacking. Third, the genome of the cancer cell is rewired and signaling networks are reprogrammed during this process of metastatic progression, either to adapt to the changing tumor microenvironment or to overcome the cytotoxicity of drugs (Hanahan and Weinberg, 2011), and biomarkers/tools that monitor any given pathway may lose significance due to the changing/evolving tumor dependency from that pathway to unknown pathway(s) (the so-called addiction switch) (Weinstein, 2002). Consequently, pathway-specific biomarkers that monitor the "known" in the setting of the so-called unknown-unknowns of tumor biology introduce bias in the short run and prove ineffective in the long run. Last, but not least, single-cell studies have shown that when stochastic, invasive, and proliferative events are triggered by perturbations (e.g., mechanical or chemical signals), each individual cell adapts on its own, i.e., cancer cells *go solo* (Chung et al., 2017; Ellsworth et al., 2017; Ferronika et al., 2017; Kimura et al., 2010; Kubota et al., 2017; Lee et al., 2014; Lorentzen et al., 2018; Ramapathiran et al., 2014; Su et al., 2017; Wu et al., 2018). Hence, any effective biomarker/assay must be sensitive enough to detect the plasticity of metastatic programming within a few sparsely distributed tumorigenic cells, i.e., cells that can metastasize and initiate new tumors at distant sites, within a large population of non-tumorigenic cells.

Despite these shortfalls, experts agree that estimating the metastatic "potential" is a problem that only molecular imaging can resolve, rather than conventional techniques, e.g., immunohistochemistry (IHC) (Winnard et al., 2008). So far, improved imaging platforms have helped detect established metastases (Frangioni, 2008) and assessed tumor cell properties as surrogate markers of metastatic potential (e.g., glucose consumption, hypoxia, angiogenesis, integrin expression patterns, or matrix metalloproteinase activities; reviewed in Winnard et al., 2008) and even visualized the metastatic process in real time *in vivo* (Sahai, 2007). However, single-cell-based assays to measure the dynamic prometastatic signaling programs that

[1]Department of Medicine, University of California at San Diego, George Palade Labs, Room 232, La Jolla, CA 92093-0651, USA

[2]Department of Cellular and Molecular Medicine, University of California at San Diego, La Jolla, CA 92093-0651, USA

[3]Moores Cancer Center, University of California, San Diego, La Jolla, CA, USA

[4]These authors contributed equally

[5]Lead Contact

*Correspondence: prghosh@ucsd.edu

https://doi.org/10.1016/j.isci.2018.11.022

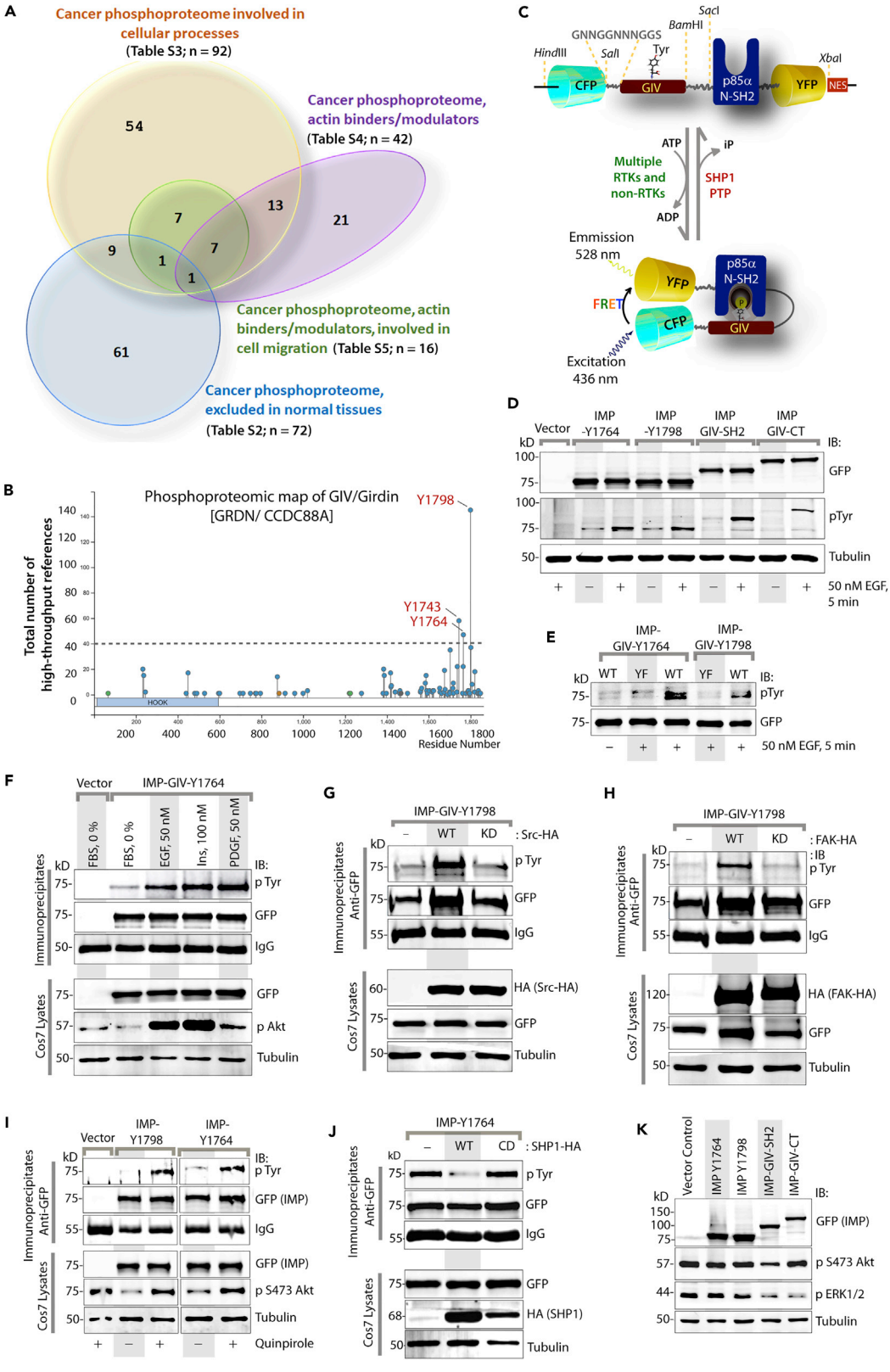
A
Cancer phosphoproteome involved in cellular processes (Table S3; n = 92)
Cancer phosphoproteome, actin binders/modulators (Table S4; n = 42)
Cancer phosphoproteome, actin binders/modulators, involved in cell migration (Table S5; n = 16)
Cancer phosphoproteome, excluded in normal tissues (Table S2; n = 72)
54
13
21
7
9
1
7
1
61
B
Phosphoproteomic map of GIV/Girdin [GRDN/ CCDC88A]
Y1798
Y1743
Y1764
Total number of high-throughput references
HOOK
Residue Number
C
GNNGGNNNGGS
HindIII
SalI
Tyr
BamHI
SacI
XbaI
CFP
GIV
p85α N-SH2
YFP
NES
ATP
iP
Multiple RTKs and non-RTKs
SHP1 PTP
ADP
Emmission 528 nm
FRET
Excitation 436 nm
D
Vector
IMP -Y1764
IMP -Y1798
IMP GIV-SH2
IMP GIV-CT
kD
IB:
GFP
pTyr
Tubulin
50 nM EGF, 5 min
E
IMP-GIV-Y1764
IMP-GIV-Y1798
WT
YF
pTyr
GFP
50 nM EGF, 5 min
F
Vector
IMP-GIV-Y1764
FBS, 0 %
FBS, 0 %
EGF, 50 nM
Ins, 100 nM
PDGF, 50 nM
Immunoprecipitates
Cos7 Lysates
p Tyr
GFP
IgG
p Akt
Tubulin
G
IMP-GIV-Y1798
WT
KD
: Src-HA
Anti-GFP
HA (Src-HA)
H
: FAK-HA
HA (FAK-HA)
I
Vector
IMP-Y1798
IMP-Y1764
GFP (IMP)
p S473 Akt
Quinpirole
J
IMP-Y1764
CD
: SHP1-HA
HA (SHP1)
K
Vector Control
IMP Y1764
IMP Y1798
IMP-GIV-SH2
IMP-GIV-CT
p S473 Akt
p ERK1/2

Figure 1. Rationale, Design, and Biochemical Validation of IMPs

(A) The pan-cancer phosphoproteome (Table S1) was analyzed with additional filters (see Transparent Methods and Tables S2, S3, S4, and S5 for list of phosphoproteins returned with each filter/criterion).

(B) Phosphoproteomic map of GIV/Girdin. Tyrosine-phosphorylated peptides are most frequently detected by high-throughput (HTP) mass spectrometry (MS) studies. Tyrosines 1764 and 1798 are known to bind and activate PI3K, whereas the role of Y1743 remains unknown.

(C) Schematic illustrating the modular makeup of IMP probes. A previously validated (Ullman et al., 1997) nuclear export signal (NES) was incorporated to retain most of the probe in the cytosolic compartment.

(D) Immunoblots showing expression and ligand-induced phosphorylation of various IMP probes in Cos7 cells after EGF stimulation.

(E) Immunoblots showing the phosphorylation status of wild-type (WT) IMP-Y1764 and Y1798 and their corresponding YF mutants after EGF stimulation.

(F) Serum-starved Cos7 cells expressing IMP-Y1764 were stimulated with various growth factors before lysis. Lysates were immunoprecipitated with anti-GFP monoclonal antibody, and tyrosine phosphorylation of IMP was analyzed by immunoblotting.

(G and H) Lysates of Cos7 cells co-expressing IMP-Y1798 and WT or kinase-dead (KD) Src-HA (G) or FAK-HA (H) were immunoprecipitated and analyzed for tyrosine phosphorylation of IMP as in (F).

(I) Lysates of Cos7 cells expressing IMP-Y1764 or Y1798 and stimulated with lysophosphatidic acid (LPA) were immunoprecipitated and analyzed for tyrosine phosphorylation of IMP as in (F).

(J) Lysates of Cos7 cells expressing IMP-Y1764 and WT or catalytically dead (CD) SHP1-HA were immunoprecipitated and analyzed for tyrosine phosphorylation of IMP as in (F).

(K) Whole-cell lysates of Cos7 cells expressing various IMP probes were analyzed for phospho(p) and total(t) Akt and ERK, tubulin, and GFP (IMPs) by immunoblotting.

contribute to the "potential" for metastasis remains a *Holy Grail*. This is largely because conventional approaches (immunofluorescence and IHC) employed to study most biomarkers on fixed tissues are fraught with technical limitations (Sato et al., 2002; Veeriah et al., 2014). Even when live cells or tissues are used in the above-mentioned approaches, one serious flaw remains, i.e., the loss of vital information pertinent to individual cells due to averaging over an ensemble of readouts (Ray, 2013). The concept of single-cell studies has gained traction in the fields of metabolomics (Zenobi, 2013) and signal transduction (Clister et al., 2015; Philips, 2005) and among cell biologists who seek to explore how cellular processes are organized and regulated *in vivo* (Midde et al., 2013), but has not been applied to study metastatic potential.

Here we report the development of fluorescence resonance energy transfer (FRET) biosensors that measure the metastatic potential of single living cancer cells by overcoming both aforementioned limitations, i.e., they account for the unknown-unknowns of an evolving tumor biology and eliminate averaging losses during conventional molecular imaging.

RESULTS

Pan-cancer Phosphoproteome Reveals that Tyrosine Phosphorylation of Girdin Is a Putative Metastasis-Related Phosphoevent

In search of an ideal target, first we carried out a comprehensive analysis of the pan-cancer phosphoproteome using the NIH-supported, continuously curated, and interactive systems biology resource, PhosphoSitePlus (Hornbeck et al., 2004, 2012, 2015) to study experimentally observed post-translational modifications in the regulation of biological processes. Using powerful gene ontology (GO)-analytical tools (PANTHER [Mi et al., 2017], GOrilla [Eden et al., 2009], and REVIGO [Supek et al., 2011]) for mining, interpreting, and visualizing this data, we noted that several pathways and biological processes were overrepresented in the pan-cancer phosphoproteome above the pan-human phosphoproteome set as reference (see Figure S1, Table S1). To identify phosphoproteins that are selectively seen in cancers, we searched for phosphopeptides that are present in cancers, but not in normal tissues. A handful of pathways (Figure S2A) and biological processes (Figures S2B and S2C) were over- or under-represented over the reference set, and only one GO term enriched over the others, i.e., negative regulators of apoptosis (Figure S2D). Because high-resolution imaging of metastasizing cancer cells has underscored the importance of actin cytoskeleton remodeling as a fundamental prerequisite for cancer invasion (Sahai, 2007), next we searched the pan-cancer phosphoproteome using a combination of different criteria for enriching for either "cellular processes" (the largest GO biological process enriched in cancer-specific phosphoproteins; S2b), actin binders/modulators and those involved in cell migration (the most important property of tumor cells that has marked effects on tumor growth, resistance, and spread [Waclaw et al., 2015]), but are excluded from normal tissues (Figure 1A; Tables S2, S3, S4, and S5). Only one phosphopeptide, pY1798, in a protein named GIV/GRDN (Gα-interacting vesicle-associated; a.k.a. Girdin; gene: *CCDC88A*) fits all the criteria.

Girdin (a.k.a, GIV, APE, HkRP1) is essentially a large, multi-modular, cytosolic signal transducer that was co-discovered by four groups nearly simultaneously (Anai et al., 2005; Enomoto et al., 2005, 2006; Simpson

et al., 2005). It has been recognized as a bona fide driver of metastasis because of its ability to enhance phosphatidylinositol 3-kinase (PI3K)-Akt signals and couple them to cytoskeletal remodeling (Takahashi et al., 2015; Weng et al., 2010), an essential feature for tumor cell invasion. Girdin also serves another role, that of a guanine nucleotide exchange modulator, which integrates signals downstream of multiple classes of receptors by coupling ligand-activated receptors to activation of trimeric GTPases (Aznar et al., 2016; DiGiacomo et al., 2018; Ghosh et al., 2017). Consequently, receptor-initiated signals are modulated by G protein intermediates (Garcia-Marcos et al., 2015). Ligand stimulation of a variety of receptors directly (as in the case of growth factor receptor tyrosine kinases [RTKs]) or indirectly (via non-RTKs, as in the case of G-protein coupled receptor [GPCRs], Toll-like receptors, integrins) trigger phosphorylation of GIV on two key tyrosines (Y1764 and Y1798) within its C terminus (Figure 1B) (Dunkel et al., 2016; Kuga et al., 2017; Lin et al., 2011; Lopez-Sanchez et al., 2015; Mizutani et al., 2018; Omori et al., 2015), which directly bind and activate Class 1 PI3Ks, and subsequently, Akt (Lin et al., 2011) (Figure S3A). Multiple groups have independently validated the role of this *multi-receotor-GIV-PI3K* axis in driving metastasis and/or enhancing prometastatic features of tumor cells across a variety of solid cancers (summarized in Ghosh, 2015; Ghosh et al., 2011; Takahashi et al., 2015; Weng et al., 2010). These studies have established causal links between GIV and several ominous traits that aid in the acquisition of metastatic potential, e.g., collective migration/invasiveness, survival, stemness, and chemoresistance (summarized in Aznar et al., 2016; Takahashi et al., 2015).

Rationale Design and Validation of FRET Probes that Measure Functional Phosphorylation of Girdin

We hypothesized that the measurement of the intensity of functional phosphorylation of GIV within the *multi-receptor-GIV-PI3K* axis in individual living cells will serve as a surrogate to assess the extent of multi-receptor-driven prometastatic signaling via the GIV-PI3K node. To achieve this goal, we designed intramolecular FRET probes with two modules (Figure 1C): (1) short stretches of GIV flanking either one or both critical tyrosines, Y1764 and Y1798 (Figure S3B) and (2) N-Src homology 2 (SH2) domain of p85α(PI3K); the former serves as a target substrate for multiple tyrosine kinases, and when phosphorylated serves as the ligand for recognition by N-SH2- p85α(PI3K). The two modules are separated by a flexible linker and sandwiched by eCFP (donor) and eYFP (acceptor) proteins, such that binding of the N-SH2- p85α(PI3K) to phosphotyrosine (pY) GIV ligand leads to folding of the probe bringing the donor and acceptor fluorescent proteins into close proximity, with resultant gain in FRET. Because these synthetic probes were built to assess multi-receptor-GIV-PI3K signaling, we named them ''integrators of metastatic potential (IMPs).''

We first validated the IMP probes biochemically by confirming that they are expressed as fluorescent-tagged proteins of expected size and that they are phosphorylated on tyrosines after ligand (epidermal growth factor [EGF]) stimulation (Figure 1D). Ligand-dependent phosphorylation was virtually abolished when the corresponding phosphorylation-deficient IMPs were expressed in which Tyr (Y) was substituted by Phe (F) (henceforth referred to as YF) (Figures 1E, S4A, and S4B). Consistent with the fact that multiple pathways converge on GIV, IMPs were phosphorylated upon stimulation with multiple growth factors (EGF, insulin, platelet-derived growth factor) (Figures 1F, S4C, and S4D), non-RTKs Src and FAK (Figures 1G, 1H, S4E, and S4F), and ligand for LPAR, a GPCR (Figure 1I). As expected, the expression of catalytically active SHP1, a protein tyrosine phosphatase that dephosphorylates GIV's tyrosines (Mittal et al., 2011), abolished tyrosine phosphorylation of IMPs (Figures 1J and S4G). Finally, because ideal biosensors do not perturb the system under test (Haugh, 2012), and isolated domains of GIV that can bind RTKs or activate G proteins can display a range of biological activity (Midde et al., 2015) and alter the ratio of Akt and ERK signals, we asked which IMP construct is the least perturbing. In the presence of a functional SH2-like or GEF module (Lin et al., 2014; Midde et al., 2015) IMP-SH2 and IMP-GIV-C-terminus (IMP-CT) constructs (shown in Figure S3B) altered the levels of Akt and ERK signals at baseline steady states, whereas under the same conditions the IMP-1764 or IMP-1798, constructs that contain merely 13 amino acids of GIV appeared inert (Figure 1K). Hence, these two minimalist IMPs were deemed appropriate for further evaluation. Consistent with their predicted inertness, overexpression of either IMP-1764 or IMP-1798 or their non-phosphorylatable YF mutants did not affect 2D migration in scratch wound assays (Figure S5). Although both Y1764 and Y1798 cooperatively activate PI3Ks, because Y1764 is a target for both RTKs and non-RTKs, whereas Y1798 is exclusively phosphorylated by non-RTKs (Lin et al., 2011), we focused heavily on IMP-1764.

Next we validated these probes in live cells to determine if ligand-induced tyrosine phosphorylation was also accompanied by intramolecular folding and FRET. FRET signals were analyzed exclusively at the

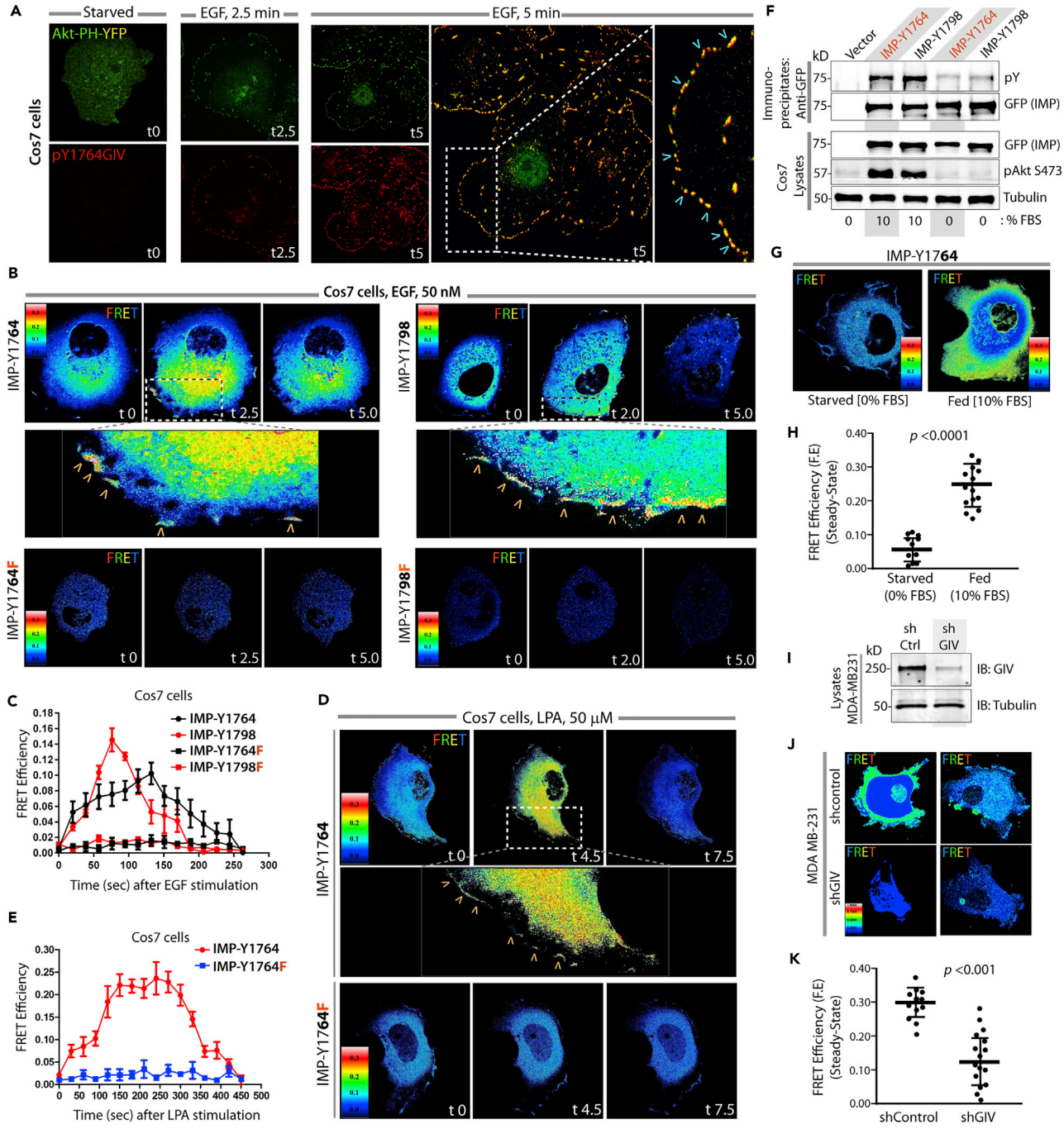

Figure 2. Validation of the IMPs using Single-Cell FRET Imaging

(A) Serum-starved Cos7 cells expressing Akt-PH-YFP (pseudocolored green) were stimulated with EGF, fixed, and stained for tyrosine-phosphorylated GIV (anti-pY1764GIV; red) and analyzed by confocal microscopy.

(B) Serum-starved Cos7 cells expressing IMP-Y1764, Y1798, or their corresponding YF mutants were stimulated with EGF and analyzed by confocal live-cell FRET imaging. Representative freeze-frame images from Videos S1, S2, S3, and S4 are shown.

(C) Time traces display the dynamic changes in FRET efficiency in (B); 12–15 cells were analyzed in 3 independent assays.

(D) Serum-starved Cos7 cells expressing IMP-Y1764 or the YF mutant were stimulated with LPA and analyzed by confocal live-cell FRET imaging. Representative freeze-frame images from Videos S5 and S6 are shown.

(E) Time traces display the dynamic changes in FRET efficiency in 12–15 cells that were analyzed in 3 independent assays.

Figure 2. *Continued*

(F) Immunoblots showing the contribution of serum (10%) on the phosphorylation status of wild-type (WT)-IMP-1764 and WT-IMP-1798 probes expressed in Cos7 cells at steady state. Phosphorylation of the IMP peptides and Akt was exclusively observed in fed state (10% FBS), but not in starved (0% FBS) conditions.

(G) Representative steady-state FRET images of Cos7 cells expressing IMP-1764 probe and its phosphorylation triggered by 10% serum. Higher FRET efficiency signals were detected in cells with 10% serum, but not in cells without serum.

(H) Scatterplots comparing the FRET efficiency at the PM in (G). Results are expressed as mean ± SD.

(I) Lysates of control and GIV-depleted MDA-MB-231 cells were analyzed for GIV depletion by immunoblotting (IB). The efficiency of depletion was estimated as ~85% by band densitometry.

(J) Representative steady-state FRET images of MDA-MB-231 cells in (I) expressing the IMP-1764 probe.

(K) Scatterplots comparing the FRET efficiency at the PM in (J). Results are expressed as mean ± SD.

plasma membrane (PM) because Class IA PI3Ks activated by tyrosine-phosphorylated GIV transduce signals primarily by phosphorylating phosphatidylinositol-4,5-bisphosphate at the PM (Engelman, 2009), and because tyrosine phosphorylation of GIV (as determined by immunofluorescence using anti-pYGIV antibody [Lopez-Sanchez et al., 2014]) coincided temporally and spatially with the activation of PI3K (as determined using the fluorescent reporter, YFP-tagged PH-domain of Akt [Lin et al., 2011]) on microdomains at the PM (Figure 2A). These temporal and spatial patterns were reproduced using IMP probes in living cells responding to either EGF (Figures 2B and 2C; Videos S1, S2, S3, and S4) or lysophosphatidic acid (LPA) (Figures 2D and 2E; Videos S5 and S6). Regardless of the pathway activated, FRET was observed at the PM within 2–2.5 min for both IMP-1764 and IMP-1798, albeit with a few notable differences. FRET at the PM was transient in the case of growth factors, whereas a more delayed (peak 4.5 min) and sustained response was seen in the case of LPA. These findings are consistent with the differential kinetics of Akt activation downstream, i.e., Akt phosphorylation typically peaks at 5 min after stimulation with growth factors, but at 15 min after stimulation of GPCRs (Garcia-Marcos et al., 2009). No FRET was observed when each IMP was substituted in the above-mentioned assays with its non-phosphorylatable YF counterpart, indicating that ligand-stimulated tyrosine phosphorylation of GIV is essential for gaining FRET in each instance. Furthermore, compared with starved (0% fetal bovine serum [FBS]) cells, increased ambient signals in serum-fed cells (10% FBS) were accompanied by a higher steady-state probe phosphorylation (Figure 2F) and FRET efficiency (F.E) (Figures 2G and 2H), indicating that IMPs can detect ambient multi-receptor-driven signal flow at a steady state without the need to acutely activate a given receptor/pathway. Furthermore, depletion of GIV in MDA-MB-231 cells, which require GIV for their ability to form lung metastases when xenografted in nude mice (Jiang et al., 2008), was accompanied by a reduction in F.E (Figures 2I–2K). Together, these findings demonstrated that IMPs are the minimal platforms that can measure the timing, intensity, and location of functional phosphorylation of GIV in living cells at steady state.

Single-Cell Imaging of Signaling through the *GIV-PI3K* Axis Reveals the Heterogeneity in Metastatic Potential and Tracks the Increasing Potential during Metastasis

Next we asked if the IMPs can measure the steady-state ambient multi-receptor signaling via the *GIV-PI3K* axis. If F.E. were to be measured at steady state, we assumed such measurement to reflect the equilibrium between the activity of multiple tyrosine kinases (i.e., forward reaction), the antagonistic dephosphorylating action of PTP and SHP1 (i.e., reverse rate reactions), and any upstream triggers to both enzymes. Hence, a high F.E observed would imply the activation of multiple pathways that trigger the prometastatic tyrosine kinase signaling pathways as well as those that suppress SHP1's protein phosphatase activity and would indicate overall hypersignaling via the TK-GIV axis. We specifically asked if such steady-state measurements can serve as a readout of the aberrant TK-GIV prometastatic signaling during the acquisition of metastatic potential. If so, we predicted that such measurement should come with three key advantages: (1) eliminate the need to know to which upstream pathways (drivers versus hitchhikers) a given tumor is addicted; (2) avoid perturbing the intrinsic pathologic pathways with extrinsic ligands that introduce undesired bias, and (3) ensure continued usefulness despite changes in tumor dependency on a given pathway, as during metastatic progression or development of drug resistance. To test these, we first validated the IMPs using three well-characterized metastatic breast and lung adenocarcinoma cell lines, MDA-MB-231, PC-9, and H2030, and their corresponding highly metastatic subclones (BrM) that were selected in mice and display ~10-fold enhanced ability to metastasize to the bone and brain (Nguyen et al., 2009; Valiente et al., 2014) (Figure S6A). Despite their diverse genetic backgrounds (Figure S6B), all BrM clones consistently displayed one common feature compared with their parental counterparts: higher Akt activity (Figures 3A–3C), whereas the patterns of immunofluorescence staining for tyrosine-phosphorylated GIV (pY1764GIV) showed only minor differences (Figure S7). Using the IMP-Y1764 probe, we found that the

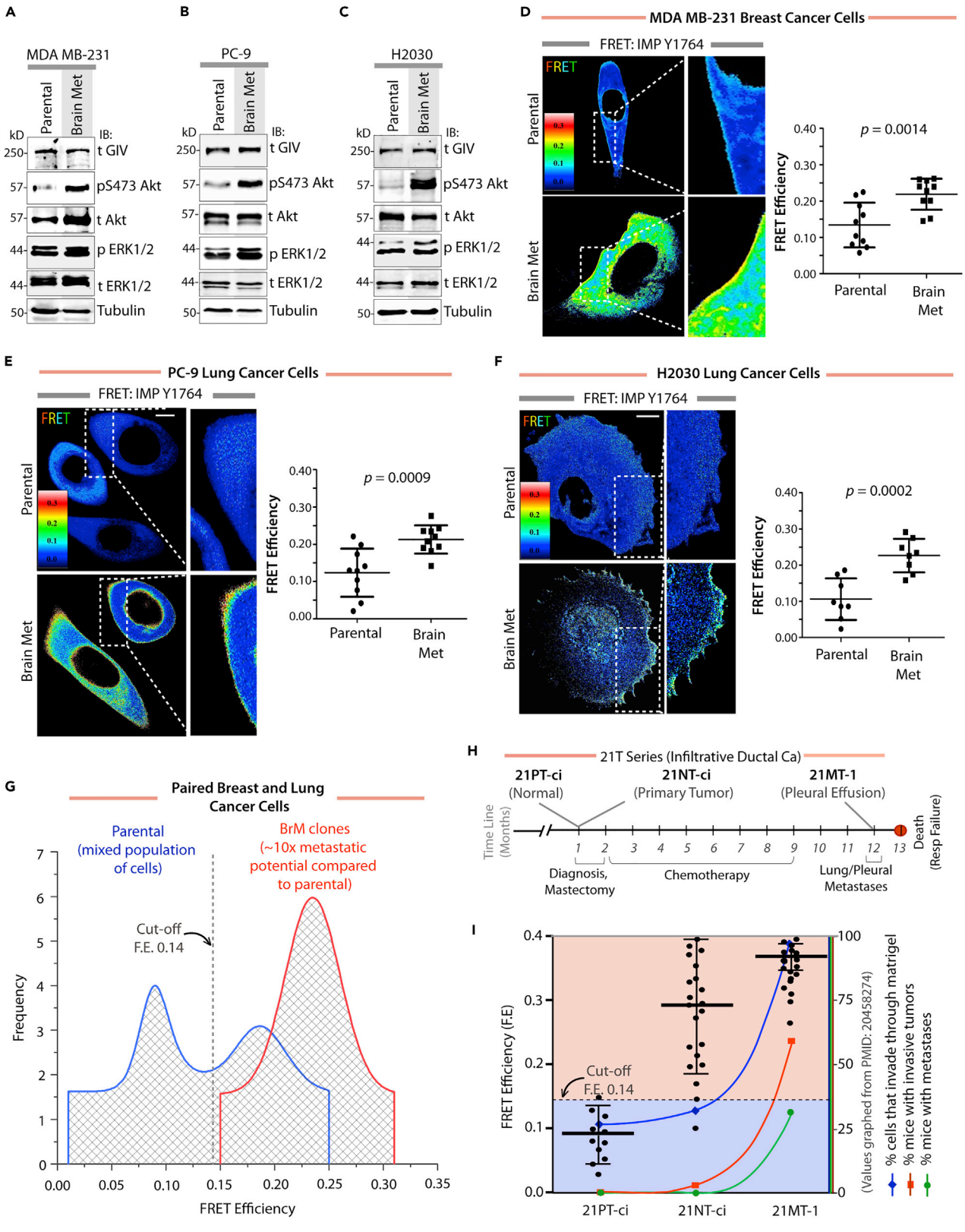
A
MDA MB-231
Parental
Brain Met
kD
IB:
250-
t GIV
57-
pS473 Akt
57-
t Akt
44-
p ERK1/2
44-
t ERK1/2
50-
Tubulin
B
PC-9
C
H2030
D
MDA MB-231 Breast Cancer Cells
FRET: IMP Y1764
FRET
Parental
Brain Met
FRET Efficiency
p = 0.0014
E
PC-9 Lung Cancer Cells
p = 0.0009
F
H2030 Lung Cancer Cells
p = 0.0002
G
Paired Breast and Lung Cancer Cells
Parental (mixed population of cells)
BrM clones (~10x metastatic potential compared to parental)
Cut-off F.E. 0.14
Frequency
FRET Efficiency
H
21T Series (Infiltrative Ductal Ca)
21PT-ci (Normal)
21NT-ci (Primary Tumor)
21MT-1 (Pleural Effusion)
Time Line (Months)
Death (Resp Failure)
Diagnosis, Mastectomy
Chemotherapy
Lung/Pleural Metastases
I
FRET Efficiency (F.E)
Cut-off F.E. 0.14
21PT-ci
21NT-ci
21MT-1
(Values graphed from PMID: 20458274)
% cells that invade through matrigel
% mice with invasive tumors
% mice with metastases

Figure 3. Steady-State FRET Imaging using IMP-Y1764 in Isogenic Cancer Cells with Variable Metastatic Potentials

(A–C) Lysates of parental MDA-MB-231(A), PC-9(B), and H2030(C) cancer cells and their brain metastatic (met) counterparts were analyzed for phospho(p) and total(t) Akt, ERK, tubulin, and GIV by immunoblotting.

(D–F) Parental and brain metastatic clones of MDA-MB-231 (D), PC-9 (E), and H2030 (F) cells expressing IMP-Y1764 were analyzed for steady-state FRET by confocal live-cell imaging. Representative FRET images (left) and scatterplots (right) comparing the FRET efficiency in parental versus brain metastatic clones are displayed. Results are expressed as mean ± SD.

(G) Gaussian fits of composite histograms comparing F.E in parental (blue) versus brain metastatic (met; red) clones of cancer cells in (D–F) are displayed.

(H) Schematic summarizing the clinical course of patient #21, the source of 21T series of normal (NT-ci), primary (PT-ci), and metastatic (MT-1) breast cancer cells (Band et al., 1990).

(I) Graphs display the average FRET efficiency (left y axis) and invasive properties (right y axis; [Souter et al., 2010]) of the 21T cell lines. Results are expressed as mean ± SD.

steady-state F.E. in individual cells varied over a range in these cells (Figures 3D–3F); the variance is in keeping with the expected heterogeneity in metastatic potential within a given population of cells (Hanahan and Weinberg, 2011). However, the mean F.E. of the BrM cells was consistently ~2-fold higher than that of their parental counterparts (Figures 3D–3F). Gaussian fits of the histograms of the FRET efficiencies of individual cells from these paired cell lines revealed that parental cells were more heterogeneous (wider spread of F.E with two peaks), whereas their BrM counterparts were less heterogeneous (a single narrow peak), and that a subset of parental cells behaved just like BrM cells (partial overlap between second peak of parental cells and the BrM cells). Because a feature of quantitative single-cell imaging is to allow the measured entity to be quantified by choosing a cutoff value for the histogram of overlap integrals, the data in Figure 3G suggest that 0.14 is a reasonable cutoff; values below or above 0.14 would indicate that the potential for metastasis is low or high, respectively. Because some cells in the parental population displayed F.E. > 0.14 and overlapped with BrM cells, these findings validate that single-cell steady-state F.E. measured using IMP-Y1764 can detect those subpopulations of parental cells that have acquired the metastatic potential, but risk being obscured by averaging (mean F.E. of parental cells = 0.125, which is below the 0.14 cutoff).

We also confirmed that the high F.E. observed in BrM cells required a phosphorylatable tyrosine within the IMP-Y1764 probe (Figures S8A and S8B) and yet did not merely reflect a generalized hyperactivation of tyrosine-based signaling (Figure S8C). Furthermore, replacement of the GIV sequence in IMP-Y1764 with a stretch of residues that flank Y941 on IRS1 (Figure S8D), which is phosphorylated by multiple RTKs and binds p85α(PI3K) (Sato et al., 2002), abolished the probe's ability to distinguish parental from their BrM counterparts (Figures S8E and S8F). These results demonstrate the functional specificity of tyrosine-phosphorylated GIV as a portal for the integration of prometastatic PI3K signaling downstream of multiple receptors; findings were not reproducible by other phosphotyrosine substrate that also serve as ligand for p85α(PI3K).

Next we interrogated the ability of the IMP-Y1764 probe to distinguish between the MCF7 and MDA-MB-231 cells, two lines frequently studied for their contrasting metastatic potential (Winnard et al., 2008). MDA-MB-231 cells express full-length GIV (Figure S9A) and metastasize at a frequency approaching ~100% (100% to LN, 40%–70% to lungs), whereas the MCF7 cells do not metastasize (Garcia-Marcos et al., 2011; Ghosh et al., 2010; Jenkins et al., 2005). We found that that the extent of phosphorylation of IMP-Y1764 (Figure S9B) and the mean F.E. in MCF7 (0.06 ± 0.01) and MDA-MB-231 cells (0.24 ± 0.05) (Figures S9C and S9D) were in keeping with their contrasting metastatic potentials. These results suggest that the IMP probe may be able to distinguish tumor cells with high metastatic potential from the others. Despite the fact that one major outcome of tyrosine phosphorylation of GIV and its ability to bind PI3K is the enhancement of Akt signals, the IMP-Y1764 probe did not capture all forms of ambient Akt signals in cells because we noted that the F.E. in MCF7 cells was low, despite high levels of Akt phosphorylation (Figure S9A). These findings suggest that F.E of IMP-Y1764 can somehow distinguish prometastatic GIV-PI3K-Akt signals from other Akt signals.

Single-Cell Imaging of Signaling through the *GIV-PI3K* Axis Maintains Its Usefulness in Tracking Metastatic Potential Despite Tumor Evolution and Onset of Chemoresistance

Next we asked if the IMP-Y1764 probe retains its ability to detect the metastatic potential of tumor cells despite evolving signaling programs and tumor biology. Such evolution is encountered under two circumstances:(1) during metastatic progression in humans and (2) during the development of drug resistance. To study the first, we used the 21T lines that were derived from the same patient during breast cancer progression (Band et al., 1990) (Figure 3H) and display an array of changing epigenetic, proteomic, and signaling programs during progressive acquisition of metastatic potential (Figure S10A). Enhanced Akt

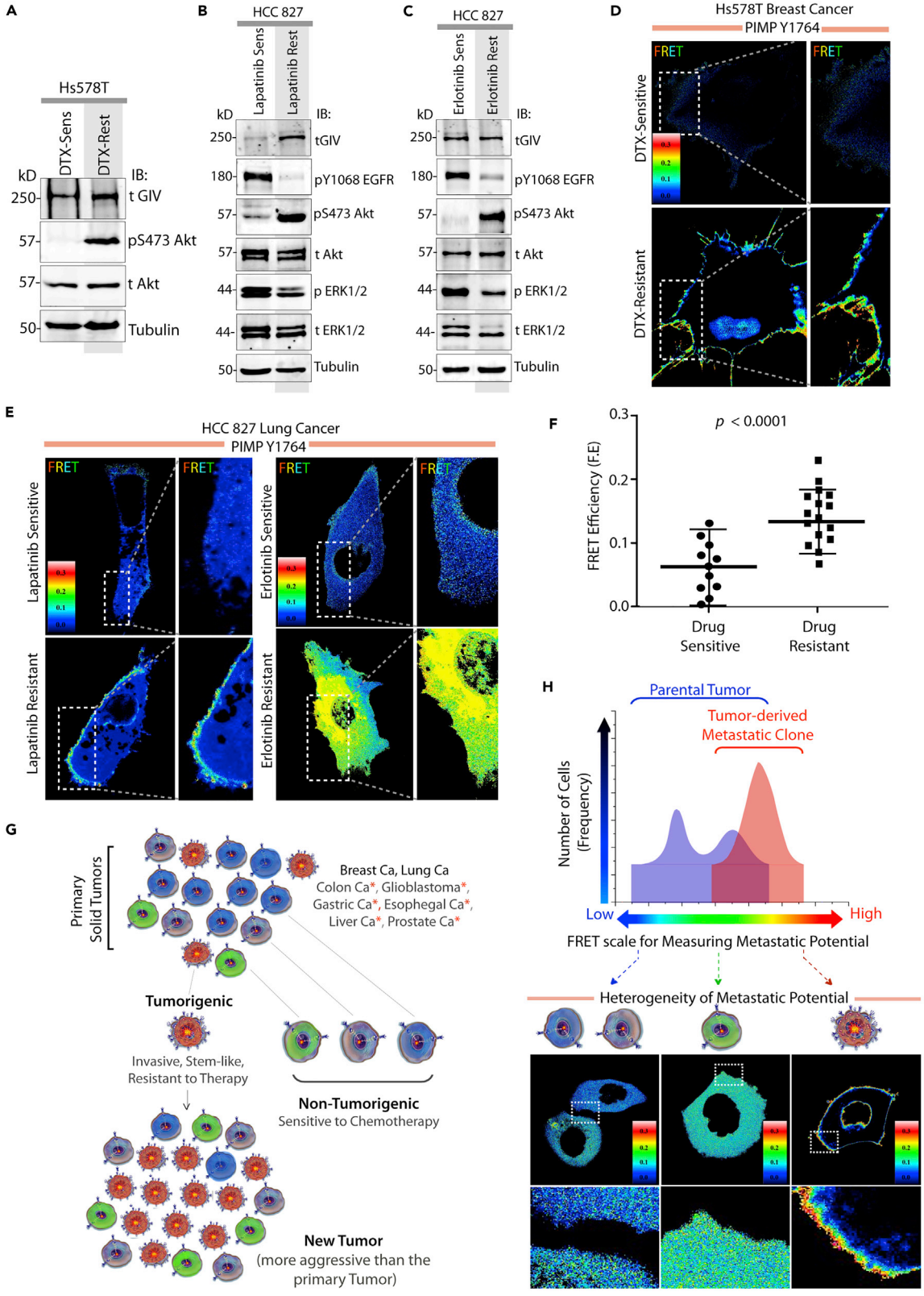
A
Hs578T
DTX-Sens
DTX-Rest
kD
IB:
250-
t GIV
57-
pS473 Akt
57-
t Akt
50-
Tubulin
B
HCC 827
Lapatinib Sens
Lapatinib Rest
kD
IB:
250-
tGIV
180-
pY1068 EGFR
57-
pS473 Akt
57-
t Akt
44-
p ERK1/2
44-
t ERK1/2
50-
Tubulin
C
HCC 827
Erlotinib Sens
Erlotinib Rest
kD
IB:
250-
tGIV
180-
pY1068 EGFR
57-
pS473 Akt
57-
t Akt
44-
p ERK1/2
44-
t ERK1/2
50-
Tubulin
D
Hs578T Breast Cancer
PIMP Y1764
FRET
FRET
DTX-Sensitive
DTX-Resistant
E
HCC 827 Lung Cancer
PIMP Y1764
FRET
FRET
FRET
FRET
Lapatinib Sensitive
Erlotinib Sensitive
Lapatinib Resistant
Erlotinib Resistant
F
p < 0.0001
FRET Efficiency (F.E)
0.3
0.2
0.1
0.0
Drug Sensitive
Drug Resistant
G
Primary Solid Tumors
Breast Ca, Lung Ca
Colon Ca*, Glioblastoma*,
Gastric Ca*, Esophegal Ca*,
Liver Ca*, Prostate Ca*
Tumorigenic
Invasive, Stem-like,
Resistant to Therapy
Non-Tumorigenic
Sensitive to Chemotherapy
New Tumor
(more aggressive than the
primary Tumor)
H
Parental Tumor
Tumor-derived
Metastatic Clone
Number of Cells
(Frequency)
Low
High
FRET scale for Measuring Metastatic Potential
Heterogeneity of Metastatic Potential

Figure 4. Steady-State FRET Imaging Using IMP-Y1764 before and after the Emergence of Drug Resistance

(A–C) Lysates of Hs578T(A) and HCC827 (B and C) cancer cells, sensitive or resistant to docetaxel (DTX), lapatinib (Lap), or erlotinib were analyzed by immunoblotting (IB).

(D–F) Sensitive and resistant Hs578T (A) and HCC827 (B and C) cancer cells expressing IMP-Y1764 were analyzed for steady-state FRET by confocal live-cell imaging. Representative FRET images and scatterplots comparing the F.E in sensitive versus resistant cells is shown. Results are expressed as mean ± SD.

(G and H) Summary of findings. Schematic (G; modified and adapted from [Wang and Dick, 2005]) showing that few tumorigenic cells are chemoresistant and account for tumor recurrence and metastasis, whereas most tumor cells are non-tumorigenic and are typically sensitive to chemotherapy. Schematic in (H) summarizes how single-cell FRET-based imaging with IMPs can detect those few cells with tumorigenic potential within the primary tumor (blue; right peak within the bimodal distribution) that are enriched later during the process of metastasis (single red peak).

signaling during metastatic progression in 21T cells (Qiao et al., 2007) has previously been shown to track well with increased expression of GIV mRNA and protein (Garcia-Marcos et al., 2011) as well as enhanced tyrosine phosphorylation of GIV at Y1764/98 (Lin et al., 2011). Here we found that F.E using the IMP-Y1764 probe was low in normal (PT-ci; 0.08 ± 0.01) but high in primary (NT-ci; 0.28 ± 0.07) and metastasized (MT-1; 0.38 ± 0.03) cells (Figures 3I and S10B), indicating that the probe could effectively categorize both NT-ci and MT-1 as cells with "high" potential for metastasis regardless of the changes in tumor biology incurred during disease progression over 1 year and cytotoxic chemotherapy received by the patient (Band et al., 1990). Furthermore, as in the case of MCF7 and MDA-MB-231 cells, the chosen cutoff F.E. of 0.14 was effective in accurately detecting the metastatic potential of 21T cells (Figure S11).

To study the impact of changing tumor biology during the acquisition of drug resistance, we used three breast and lung cancer lines (Figures S12A and 4A–4C) with variable resistance to cytotoxic chemotherapy (docetaxel) or inhibitors of RTKs (erlotinib and lapatinib). Compared with the sensitive clones, both pY1764GIV (Figure S12B) and Akt phosphorylations (Figures 4A–4C) were consistently enhanced and their expressions were upregulated in their resistant counterparts. This is in keeping with the fact that invasiveness/epithelial-mesenchymal transition (EMT) and stemness, two features of drug resistance, are both modulated by GIV (Singh and Settleman, 2010). The F.E measured using IMP-Y1764 was similarly elevated ~2- to 3-fold in the resistant clones (Figures 4D–4F), indicating that the probe accurately detected the acquisition of higher metastatic potential that coincides with drug resistance. Such detection was possible regardless of the unknown-unknowns of evolving tumor biology during the acquisition of resistance (Figure S12A).

In conclusion, IMP-Y1764 features three properties that make it ideal for molecular imaging: (1) a unique target, i.e., GIV, whose functional phosphorylation broadly reflects the intensity of convergent signaling from multiple upstream pathways via the prometastatic PI3K-Akt pathway; (2) usefulness in a FRET-based approach that retains single-cell information; and (3) ability to fulfill an urgent and unmet need, i.e., measure metastatic potential in a sensitive, specific, objective, and unbiased way by overcoming the limitations of the unknown (Figures 4G and 4H). That IMP-Y1764 detected the "high" potential for metastasis of 21T-NT-ci cells at diagnosis and 1 year before metastasis to the lungs/pleura (Band et al., 1990) suggests that F.E readouts using the IMP-Y1764 probe and the cutoff of 0.14 may be further developed for use *ex vivo* or *in vitro* in assays investigating personalized cancer therapeutic response, such that the sensitivity of any tumor to any small molecule will be studied specifically against those cells with the highest metastatic proclivity in any given tumor.

DISCUSSION

One key goal of the National Cancer Institute's Precision Medicine Initiative focuses on the development of new tools to tailor cancer therapy to the disease status and risk of metastasis—patients at high risk for metastatic disease would receive aggressive, frequently molecularly targeted therapy, whereas those with low risk for metastatic disease would be treated with appropriate local therapies, sparing them toxic side effects of therapy while maintaining high likelihood for cure. One of the main challenges preventing the implementation of precision medicine for metastasis is the limited understanding of signaling molecules and pathways that confer high metastatic potential to a small subset of cancer cells, the so-called unique subset of cancer cells, designated as metastasis-initiating cells (MICs) within a larger, heterogeneous tumor. The identity of MICs remains largely unknown, which poses two critical challenges for cancer therapy. (1) Development of drugs to block metastasis: The ability of disseminated cancer cells to produce clinically evident metastases defines a central bottleneck in disease progression. Targeting key drivers of this process represents an ideal opportunity to stop metastatic disease, even for malignant cells that disseminated before the detection of a primary tumor. (2) Stratification of patients for treatment: Only a subpopulation of patients with cancer develop metastases. Lack of reliable markers to identify MICs and patients at high risk for metastasis leads to over-treatment, causing toxic side effects without benefit to a patient.

Identifying MICs remains daunting because of the molecular heterogeneity of cancer cells, uncertainty about what molecules and signaling pathways confer metastatic potential, and dynamic re-wiring of signaling during metastasis. Detection of MICs as a biomarker for risk of metastasis offers the potential to advance cancer research, drug discovery and development, and patient care.

Our major accomplishment here is that we have engineered IMP biosensors that can detect and measure the metastatic "*potential*" of single living cancer cells (presumably any type of cancer) at a steady state. However, perhaps more importantly, we provided evidence that these biosensors can do so while remaining agnostic to the numerous unknown-unknowns of the tumor's biology, such as any genetic aberration or the epigenetic aberrations of any specific ligand/pathway. Consequently, these sensors maintain their effectiveness despite the evolving changes in the tumor cells during the natural progression of disease, or during progression under the selection pressure of anti-cancer therapies. Thus, our findings provide proof of concept that the IMP biosensors can measure the diversity and plasticity of metastatic potential of tumor cells in a sensitive and unbiased way, and in doing so, may serve as effective tools to visualize, track, and enrich (by sorting) the MICs.

LIMITATIONS OF THE STUDY AND FUTURE DIRECTIONS

Despite our success in validation of the IMP probes in cultured tumor cells, further evolution of the probes is a must before they can be used for *in vivo* imaging studies (e.g., use of better fluorophores for deep tissue imaging explants in nude mice). Because the signaling event (tyrosine phosphorylation of GIV) specifically localizes to focal adhesions, it may be critical that any sorting-related application does so while maintaining cell-extra-cellular matrix (ECM) interactions. Despite our use of OxyFluor to minimize reactive oxygen species (ROS)-induced photobleaching, it is possible that increased ROS production in tumor cells affect either the signaling pathways monitored with IMPs or the IMP probes themselves, or both. Finally, the commonly used dimerization-preventing mutation (A206K) was not present in IMPs (see details in Methods). Because on and off rate balance in IMPs at steady state critically depends on the intramolecular affinities of fluorescent proteins (FPs), any further optimization of the IMPs (either by design, or change in FPs, or based on the proposed mode of use, i.e., at steady state versus after an acute stimuli) will require considering how these rates may affect readouts. Such optimization and thoughtful considerations are warranted because successful validation of tools to detect MICs will be a transformative advance for cancer cell biology. For example, IMPs could be adapted and evolved for the development of an imaging-based *ex vivo* screening platform for assessing the effectiveness of anti-cancer drugs in killing the MICs within any tumor type; they could define quantitative metrics for activation of GIV that correlates with metastatic potential, providing the foundation needed to advance GIV as a prognostic biomarker for metastasis and potential drug target to eliminate MICs. Ultimately, these efforts could enable the clinical implementation of precision cancer therapy to improve the treatment and quality of life for patients.

METHODS

All methods can be found in the accompanying Transparent Methods supplemental file.

SUPPLEMENTAL INFORMATION

Supplemental Information includes Transparent Methods, 12 figures, 5 tables, and 6 videos can be found with this article online at https://doi.org/10.1016/j.isci.2018.11.022.

ACKNOWLEDGMENTS

We thank Gordon N. Gill and Marilyn G. Farquhar (UCSD) and Gary D. Luker and Kathryn Luker (University of Michigan) for their critical input during the preparation of the manuscript. We thank Frank Furnari (Ludwig's Cancer Institute) and Joan Massague for cell lines and reagents they shared as generous gifts. This work was supported by National Institutes of Health (NIH) grants CA100768, CA160911, and DK099226 (to P.G.). P.G. was also supported by the American Cancer Society (ACS-IRG 70-002) and by Padres Pedal the Cause/C3 (#PTC, 2017) pilot grant award and Moores Cancer Center intramural funding.

AUTHOR CONTRIBUTIONS

N.N.S cloned and generated all constructs used in this work and characterized them biochemically. K.M, H.D and L.J carried out all FRET based studies showcased here. C.R and P.G performed all bioinformatic

analysis of normal and pan-cancer phosphoproteomic datasets. K.M and P.G conceived the project. C.R and P.G wrote and edited the manuscript. P.G supervised and funded the project.

DECLARATION OF INTERESTS

P.G. has a pending patent application related to the discovery of IMP probes.

Received: July 16, 2018
Revised: September 23, 2018
Accepted: November 12, 2018
Published: December 21, 2018

REFERENCES

Anai, M., Shojima, N., Katagiri, H., Ogihara, T., Sakoda, H., Onishi, Y., Ono, H., Fujishiro, M., Fukushima, Y., Horike, N., et al. (2005). A novel protein kinase B (PKB)/AKT-binding protein enhances PKB kinase activity and regulates DNA synthesis. J. Biol. Chem. *280*, 18525–18535.

Aznar, N., Kalogriopoulos, N., Midde, K.K., and Ghosh, P. (2016). Heterotrimeric G protein signaling via GIV/Girdin: breaking the rules of engagement, space, and time. Bioessays *38*, 379–393.

Band, V., Zajchowski, D., Swisshelm, K., Trask, D., Kulesa, V., Cohen, C., Connolly, J., and Sager, R. (1990). Tumor progression in four mammary epithelial cell lines derived from the same patient. Cancer Res. *50*, 7351–7357.

Chung, W., Eum, H.H., Lee, H.O., Lee, K.M., Lee, H.B., Kim, K.T., Ryu, H.S., Kim, S., Lee, J.E., Park, Y.H., et al. (2017). Single-cell RNA-seq enables comprehensive tumour and immune cell profiling in primary breast cancer. Nat. Commun. *8*, 15081.

Clister, T., Mehta, S., and Zhang, J. (2015). Single-cell analysis of G-protein signal transduction. J. Biol. Chem. *290*, 6681–6688.

DiGiacomo, V., Marivin, A., and Garcia-Marcos, M. (2018). When Heterotrimeric G proteins are not activated by G protein-coupled receptors: structural insights and evolutionary conservation. Biochemistry *57*, 255–257.

Dunkel, Y., Diao, K., Aznar, N., Swanson, L., Liu, L., Zhu, W., Mi, X.Y., and Ghosh, P. (2016). Prognostic impact of total and tyrosine phosphorylated GIV/Girdin in breast cancers. FASEB J. *30*, 3702–3713.

Eden, E., Navon, R., Steinfeld, I., Lipson, D., and Yakhini, Z. (2009). GOrilla: a tool for discovery and visualization of enriched GO terms in ranked gene lists. BMC Bioinformatics *10*, 48.

Ellsworth, D.L., Blackburn, H.L., Shriver, C.D., Rabizadeh, S., Soon-Shiong, P., and Ellsworth, R.E. (2017). Single-cell sequencing and tumorigenesis: improved understanding of tumor evolution and metastasis. Clin. Transl. Med. *6*, 15.

Engelman, J.A. (2009). Targeting PI3K signalling in cancer: opportunities, challenges and limitations. Nat. Rev. Cancer *9*, 550–562.

Enomoto, A., Murakami, H., Asai, N., Morone, N., Watanabe, T., Kawai, K., Murakumo, Y., Usukura, J., Kaibuchi, K., and Takahashi, M. (2005). Akt/PKB regulates actin organization and cell motility via Girdin/APE. Dev. Cell *9*, 389–402.

Enomoto, A., Ping, J., and Takahashi, M. (2006). Girdin, a novel actin-binding protein, and its family of proteins possess versatile functions in the Akt and Wnt signaling pathways. Ann. N. Y. Acad. Sci. *1086*, 169–184.

Ferronika, P., van den Bos, H., Taudt, A., Spierings, D.C.J., Saber, A., Hiltermann, T.J.N., Kok, K., Porubsky, D., van der Wekken, A.J., Timens, W., et al. (2017). Copy number alterations assessed at the single-cell level revealed mono- and polyclonal seeding patterns of distant metastasis in a small-cell lung cancer patient. Ann. Oncol. *28*, 1668–1670.

Frangioni, J.V. (2008). New technologies for human cancer imaging. J. Clin. Oncol. *26*, 4012–4021.

Garcia-Marcos, M., Ghosh, P., and Farquhar, M.G. (2009). GIV is a nonreceptor GEF for G alpha i with a unique motif that regulates Akt signaling. Proc. Natl. Acad. Sci. U S A *106*, 3178–3183.

Garcia-Marcos, M., Ghosh, P., and Farquhar, M.G. (2015). GIV/Girdin transmits signals from multiple receptors by triggering trimeric G protein activation. J. Biol. Chem. *290*, 6697–6704.

Garcia-Marcos, M., Jung, B.H., Ear, J., Cabrera, B., Carethers, J.M., and Ghosh, P. (2011). Expression of GIV/Girdin, a metastasis-related protein, predicts patient survival in colon cancer. FASEB J. *25*, 590–599.

Ghosh, P. (2015). Heterotrimeric G proteins as emerging targets for network based therapy in cancer: end of a long futile campaign striking heads of a Hydra. Aging (Albany NY) *7*, 469–474.

Ghosh, P., Beas, A.O., Bornheimer, S.J., Garcia-Marcos, M., Forry, E.P., Johannson, C., Ear, J., Jung, B.H., Cabrera, B., Carethers, J.M., et al. (2010). A G{alpha}i-GIV molecular complex binds epidermal growth factor receptor and determines whether cells migrate or proliferate. Mol. Biol. Cell *21*, 2338–2354.

Ghosh, P., Garcia-Marcos, M., and Farquhar, M.G. (2011). GIV/Girdin is a rheostat that fine-tunes growth factor signals during tumor progression. Cell Adh. Migr. *5*, 237–248.

Ghosh, P., Rangamani, P., and Kufareva, I. (2017). The GAPs, GEFs, GDIs and...now, GEMs: new kids on the heterotrimeric G protein signaling block. Cell Cycle *16*, 607–612.

Hanahan, D., and Weinberg, R.A. (2011). Hallmarks of cancer: the next generation. Cell *144*, 646–674.

Haugh, J.M. (2012). Live-cell fluorescence microscopy with molecular biosensors: what are we really measuring? Biophys. J. *102*, 2003–2011.

Hornbeck, P.V., Chabra, I., Kornhauser, J.M., Skrzypek, E., and Zhang, B. (2004). PhosphoSite: a bioinformatics resource dedicated to physiological protein phosphorylation. Proteomics *4*, 1551–1561.

Hornbeck, P.V., Kornhauser, J.M., Tkachev, S., Zhang, B., Skrzypek, E., Murray, B., Latham, V., and Sullivan, M. (2012). PhosphoSitePlus: a comprehensive resource for investigating the structure and function of experimentally determined post-translational modifications in man and mouse. Nucleic Acids Res. *40*, D261–D270.

Hornbeck, P.V., Zhang, B., Murray, B., Kornhauser, J.M., Latham, V., and Skrzypek, E. (2015). PhosphoSitePlus, 2014: mutations, PTMs and recalibrations. Nucleic Acids Res. *43*, D512–D520.

Jenkins, D.E., Hornig, Y.S., Oei, Y., Dusich, J., and Purchio, T. (2005). Bioluminescent human breast cancer cell lines that permit rapid and sensitive in vivo detection of mammary tumors and multiple metastases in immune deficient mice. Breast Cancer Res. *7*, R444–R454.

Jiang, P., Enomoto, A., Jijiwa, M., Kato, T., Hasegawa, T., Ishida, M., Sato, T., Asai, N., Murakumo, Y., and Takahashi, M. (2008). An actin-binding protein Girdin regulates the motility of breast cancer cells. Cancer Res. *68*, 1310–1318.

Kimura, H., Hayashi, K., Yamauchi, K., Yamamoto, N., Tsuchiya, H., Tomita, K., Kishimoto, H., Bouvet, M., and Hoffman, R.M. (2010). Real-time imaging of single cancer-cell dynamics of lung metastasis. J. Cell Biochem. *109*, 58–64.

Kubota, S.I., Takahashi, K., Nishida, J., Morishita, Y., Ehata, S., Tainaka, K., Miyazono, K., and Ueda, H.R. (2017). Whole-body profiling of cancer metastasis with single-cell resolution. Cell Rep. *20*, 236–250.

Kuga, D., Ushida, K., Mii, S., Enomoto, A., Asai, N., Nagino, M., Takahashi, M., and Asai, M. (2017). Tyrosine phosphorylation of an actin-binding protein girdin specifically marks tuft cells in human and mouse gut. J. Histochem. Cytochem. *65*, 347–366.

Lee, M.C., Lopez-Diaz, F.J., Khan, S.Y., Tariq, M.A., Dayn, Y., Vaske, C.J., Radenbaugh, A.J., Kim, H.J., Emerson, B.M., and Pourmand, N. (2014). Single-cell analyses of transcriptional heterogeneity during drug tolerance transition in cancer cells by RNA sequencing. Proc. Natl. Acad. Sci. U S A *111*, E4726–E4735.

Lin, C., Ear, J., Midde, K., Lopez-Sanchez, I., Aznar, N., Garcia-Marcos, M., Kufareva, I., Abagyan, R., and Ghosh, P. (2014). Structural basis for activation of trimeric Gi proteins by multiple growth factor receptors via GIV/Girdin. Mol. Biol. Cell *25*, 3654–3671.

Lin, C., Ear, J., Pavlova, Y., Mittal, Y., Kufareva, I., Ghassemian, M., Abagyan, R., Garcia-Marcos, M., and Ghosh, P. (2011). Tyrosine phosphorylation of the Galpha-interacting protein GIV promotes activation of phosphoinositide 3-kinase during cell migration. Sci. Signal. *4*, ra64.

Lopez-Sanchez, I., Dunkel, Y., Roh, Y.S., Mittal, Y., De Minicis, S., Muranyi, A., Singh, S., Shanmugam, K., Aroonsakool, N., Murray, F., et al. (2014). GIV/Girdin is a central hub for profibrogenic signalling networks during liver fibrosis. Nat. Commun. *5*, 4451.

Lopez-Sanchez, I., Kalogriopoulos, N., Lo, I.C., Kabir, F., Midde, K.K., Wang, H., and Ghosh, P. (2015). Focal adhesions are foci for tyrosine-based signal transduction via GIV/Girdin and G proteins. Mol. Biol. Cell *26*, 4313–4324.

Lorentzen, A., Becker, P.F., Kosla, J., Saini, M., Weidele, K., Ronchi, P., Klein, C., Wolf, M.J., Geist, F., Seubert, B., et al. (2018). Single cell polarity in liquid phase facilitates tumour metastasis. Nat. Commun. *9*, 887.

McAllister, S.S., and Weinberg, R.A. (2014). The tumour-induced systemic environment as a critical regulator of cancer progression and metastasis. Nat. Cell Biol. *16*, 717–727.

Mi, H., Huang, X., Muruganujan, A., Tang, H., Mills, C., Kang, D., and Thomas, P.D. (2017). PANTHER version 11: expanded annotation data from Gene Ontology and Reactome pathways, and data analysis tool enhancements. Nucleic Acids Res. *45*, D183–D189.

Midde, K., Rich, R., Marandos, P., Fudala, R., Li, A., Gryczynski, I., and Borejdo, J. (2013). Comparison of orientation and rotational motion of skeletal muscle cross-bridges containing phosphorylated and dephosphorylated myosin regulatory light chain. J. Biol. Chem. *288*, 7012–7023.

Midde, K.K., Aznar, N., Laederich, M.B., Ma, G.S., Kunkel, M.T., Newton, A.C., and Ghosh, P. (2015). Multimodular biosensors reveal a novel platform for activation of G proteins by growth factor receptors. Proc. Natl. Acad. Sci. U S A *112*, E937–E946.

Mittal, Y., Pavlova, Y., Garcia-Marcos, M., and Ghosh, P. (2011). Src homology domain 2-containing protein-tyrosine phosphatase-1 (SHP-1) binds and dephosphorylates G(alpha)-interacting, vesicle-associated protein (GIV)/Girdin and attenuates the GIV-phosphatidylinositol 3-kinase (PI3K)-Akt signaling pathway. J. Biol. Chem. *286*, 32404–32415.

Mizutani, Y., Kuga, D., Iida, M., Ushida, K., Takagi, T., Tokita, Y., Takahashi, M., and Asai, M. (2018). Use of anti-phospho-girdin antibodies to visualize intestinal tuft cells in free-floating mouse jejunum cryosections. J. Vis. Exp. 57475–57480.

Nguyen, D.X., Chiang, A.C., Zhang, X.H., Kim, J.Y., Kris, M.G., Ladanyi, M., Gerald, W.L., and Massague, J. (2009). WNT/TCF signaling through LEF1 and HOXB9 mediates lung adenocarcinoma metastasis. Cell *138*, 51–62.

Omori, K., Asai, M., Kuga, D., Ushida, K., Izuchi, T., Mii, S., Enomoto, A., Asai, N., Nagino, M., and Takahashi, M. (2015). Girdin is phosphorylated on tyrosine 1798 when associated with structures required for migration. Biochem. Biophys. Res. Commun. *458*, 934–940.

Philips, M.R. (2005). Teaching resources. Imaging signal transduction in living cells with fluorescent proteins. Sci. STKE *2005*, tr28.

Qiao, M., Iglehart, J.D., and Pardee, A.B. (2007). Metastatic potential of 21T human breast cancer cells depends on Akt/protein kinase B activation. Cancer Res. *67*, 5293–5299.

Ramapathiran, L., Bernas, T., Walter, F., Williams, L., Dussmann, H., Concannon, C.G., and Prehn, J.H. (2014). Single-cell imaging of the heat-shock response in colon cancer cells suggests that magnitude and length rather than time of onset determines resistance to apoptosis. J. Cell Sci. *127*, 609–619.

Ray, L.B. (2013). Single-cell biology. Cells go solo. Introduction. Science *342*, 1187.

Sahai, E. (2007). Illuminating the metastatic process. Nat. Rev. Cancer *7*, 737–749.

Sato, M., Ozawa, T., Inukai, K., Asano, T., and Umezawa, Y. (2002). Fluorescent indicators for imaging protein phosphorylation in single living cells. Nat. Biotechnol. *20*, 287–294.

Simpson, F., Martin, S., Evans, T.M., Kerr, M., James, D.E., Parton, R.G., Teasdale, R.D., and Wicking, C. (2005). A novel hook-related protein family and the characterization of hook-related protein 1. Traffic *6*, 442–458.

Singh, A., and Settleman, J. (2010). EMT, cancer stem cells and drug resistance: an emerging axis of evil in the war on cancer. Oncogene *29*, 4741–4751.

Souter, L.H., Andrews, J.D., Zhang, G., Cook, A.C., Postenka, C.O., Al-Katib, W., Leong, H.S., Rodenhiser, D.I., Chambers, A.F., and Tuck, A.B. (2010). Human 21T breast epithelial cell lines mimic breast cancer progression in vivo and in vitro and show stage-specific gene expression patterns. Lab. Invest. *90*, 1247–1258.

Su, Y., Wei, W., Robert, L., Xue, M., Tsoi, J., Garcia-Diaz, A., Homet Moreno, B., Kim, J., Ng, R.H., Lee, J.W., et al. (2017). Single-cell analysis resolves the cell state transition and signaling dynamics associated with melanoma drug-induced resistance. Proc. Natl. Acad. Sci. U S A *114*, 13679–13684.

Supek, F., Bosnjak, M., Skunca, N., and Smuc, T. (2011). REVIGO summarizes and visualizes long lists of gene ontology terms. PLoS One *6*, e21800.

Takahashi, M., Asai, N., and Enomoto, A. (2015). Akt-Girdin as oncotarget. Oncoscience *2*, 811–812.

Ullman, K.S., Powers, M.A., and Forbes, D.J. (1997). Nuclear export receptors: from importin to exportin. Cell *90*, 967–970.

Valiente, M., Obenauf, A.C., Jin, X., Chen, Q., Zhang, X.H., Lee, D.J., Chaft, J.E., Kris, M.G., Huse, J.T., Brogi, E., et al. (2014). Serpins promote cancer cell survival and vascular co-option in brain metastasis. Cell *156*, 1002–1016.

Veeriah, S., Leboucher, P., de Naurois, J., Jethwa, N., Nye, E., Bunting, T., Stone, R., Stamp, G., Calleja, V., Jeffrey, S.S., et al. (2014). High-throughput time-resolved FRET reveals Akt/PKB activation as a poor prognostic marker in breast cancer. Cancer Res. *74*, 4983–4995.

Waclaw, B., Bozic, I., Pittman, M.E., Hruban, R.H., Vogelstein, B., and Nowak, M.A. (2015). A spatial model predicts that dispersal and cell turnover limit intratumour heterogeneity. Nature *525*, 261–264.

Wang, J.C., and Dick, J.E. (2005). Cancer stem cells: lessons from leukemia. Trends Cell Biol. *15*, 494–501.

Weinstein, I.B. (2002). Cancer. Addiction to oncogenes–the Achilles heal of cancer. Science *297*, 63–64.

Weng, L., Enomoto, A., Ishida-Takagishi, M., Asai, N., and Takahashi, M. (2010). Girding for migratory cues: roles of the Akt substrate Girdin in cancer progression and angiogenesis. Cancer Sci. *101*, 836–842.

Winnard, P.T., Jr., Pathak, A.P., Dhara, S., Cho, S.Y., Raman, V., and Pomper, M.G. (2008). Molecular imaging of metastatic potential. J. Nucl. Med. *49 Suppl 2*, 96S–112S.

Wu, H., Chen, S., Yu, J., Li, Y., Zhang, X.Y., Yang, L., Zhang, H., Hou, Q., Jiang, M., Brunicardi, F.C., et al. (2018). Single-cell transcriptome analyses reveal molecular signals to intrinsic and acquired paclitaxel resistance in esophageal squamous cancer cells. Cancer Lett. *420*, 156–167.

Zenobi, R. (2013). Single-cell metabolomics: analytical and biological perspectives. Science *342*, 1243259.

ISCI, Volume *10*

Supplemental Information

Single-Cell Imaging of Metastatic Potential of Cancer Cells

Krishna Midde, Nina Sun, Cristina Rohena, Linda Joosen, Harsharan Dhillon, and Pradipta Ghosh

TRANSPARENT METHODS:

Reagents and Antibodies: All reagents used in this study are of research grade and obtained from Sigma-Aldrich (St. Louis, MO) unless otherwise specified. Cell culture media were purchased from Invitrogen (Carlsbad, CA). EGF (Invitrogen), Insulin (Novagen), Lysophosphatidic Acid (LPA) (Sigma) and PDGF (Invitrogen) were obtained commercially. The Src inhibitor PP2 was obtained from Calbiochem. Receptor Tyrosine Kinase inhibitors Erlotinib (ChemieTek, Indianapolis, IN. Cat # CT-EL002) and Lapatinib (LC laboratories. Cat # L-4899) drugs were generously donated by Frank Furnari (Ludwig Cancer Institute - UCSD). Docetaxel was commercially obtained from Sigma Aldrich (cat # 01885). Mouse monoclonal antibodies against pTyr (BD Biosciences, cat # 610000), GFP (Santa Cruz Biotechnology), HA (Covance), total (t)ERK (Cell Signaling) and tubulin (Sigma) were purchased from commercial sources. Rabbit polyclonal antibodies against GIV-CT (Girdin T-13, Santa Cruz Biotechnology), phospho-Akt S473 (Cell Signaling), and phospho-ERK 1/2 (Cell Signaling) were obtained commercially. Rabbit monoclonal antibodies against pY1068 EGFR and total (t)Akt were obtained from Cell Signaling and anti-pY1764 GIV antibodies were obtained from Spring Biosciences (Lopez-Sanchez et al., 2014). Anti-mouse and anti-rabbit Alexa-594- and Alexa-488-coupled goat secondary antibodies were used for immunofluorescence. Goat anti-rabbit and goat anti-mouse Alexa Fluor 680 or IRDye 800 F(ab')2 for immunoblotting were from Li-COR Biosciences (Lincoln, NE). Rabbit or mouse IgGs used as negative controls in immunoprecipitation was purchased from BioRad (Hercules, CA) and Sigma (St. Louis, MO), respectively.

Plasmid Constructs: IMP-FRET probes encoding different stretches of GIV's C-terminus encompassing either one or both critical tyrosines, Y1764 and Y1798 of GIV were generated using the cloning strategy previously described for the '*phocus-2nes'* FRET probe that was used to measure functional phosphorylation of the adaptor protein IRS-1 (Sato et al., 2002). Briefly, fragment cDNAs of mutant ECFP (mutations are F64L, S65T, Y66W, N146I, M153T, V163A and N212K), mutant EYFP (mutations are S65G, V68L, Q69K, S72A and T203Y), various stretches of substrate domain from human GIV (Accession# BAE44387; see **Fig S3b**), phosphorylation recognition domain [the N-terminal SH2 domain, residues 330-429 from the p85α subunit of bovine PI3K (Accession# NM_174575), which is reported to bind both critical tyrosines within GIV's C-terminus (Lin et al., 2011)] were generated by standard PCR and cloned into the restriction sites shown in **Fig 1c**. A nuclear-export signal sequence (NES) – LPPLERLTL (Ullman et al., 1997), was inserted to retain the IMP probe in cytosol. Amino acid sequences of flexible linker LnL10 and LnL20 are GNNGGNGGSNNGGNNGNGG and GNNGGNGGSNNGNGGNGNNGGNNGNGG, respectively. Various IMP constructs, as illustrated in **Fig S3b**, were subcloned between HindIII and XbaI sites of pcDNA 3.1(+) vector (Invitrogen Co., Carlsbad, CA) using Fast Cloning Technique (Li et al., 2011). There are two noteworthy specifics in our chosen paired fluorophores: 1) Q69K mutation in eYFP: Q69 is fairly close to the chromophore anion inside the β-barrel of YFP. It was previously reported that Q69K could promote the anionic form of the chromophore to hinder its protonation, and therefore reduce the apparent pK_a to 6.1, with little effect on its other sensitivities (Griesbeck et al., 2001). 2) The commonly used dimerization preventing mutation (A206K) was not present in our construct. Prior work has carefully documented that this mutation renders probes that require conformational changes to monitor dynamic signaling events non-functional because such conformational changes depend on the weak dimerization, and yet, does not produce significant artifacts of intermolecular dimerization-related FRET (Jost et al., 2008; Kotera et al., 2010). The sequences of primers that were used for cloning IMP constructs are available upon request. GFP-Akt-PH was obtained from R. Tsien (UCSD) and previously used as a reporter to study GIV-dependent activation of PI3K in cells (Lin et al., 2011). C-terminal HA-tagged c-Src for mammalian expression was generated by cloning the entire coding sequence into pcDNA 3.1 between Xho I and Eco RI. HA tagged SHP-1 was used and validated previously (Mittal et al., 2011). All constructs were checked by DNA sequencing prior to their use in various assays.

Cell Lines: MDA-MB-231, PC-9 and H2030 parental and their brain metastatic (BrM) counterparts listed in **Fig. S5b** were generous gifts from Joan Massagué (Memorial Sloan Kettering Cancer Center, New York). Briefly, metastatic cells were isolated from either lymph node or pleural effusions of cancer patients and selected in nude mice to

generate the BrM subclones, which are known to exhibit higher invasiveness and metastatic proclivity to brain and bone (Nguyen et al., 2009; Valiente et al., 2014). The 21T series (16N, NT and MT2) cancer cell lines isolated from different stages of breast cancer progression were generous gifts from Arthur B. Pardee (Dana-Farber Cancer Institute, Harvard Medical School) and cultured as described earlier (Garcia-Marcos et al., 2011; Souter et al., 2010). Hs578T cells were obtained from ATCC, and their Docetaxel-resistant subclones were generated according to the protocol developed by Andrew C. Schofield et al (Brown et al., 2004). Briefly, cells were exposed to incremental concentrations of sub-lethal doses of docetaxel on a daily-basis for 1 hr, followed by splitting and recovery until stable revival of growth in media with drug concentration of 30 μM was achieved. Erlotinib and Lapatinib resistant HCC827 were generous gifts from Frank Furnari (Ludwig Cancer Institute – UCSD). Unless mentioned otherwise, cell lines used in this work were cultured according to ATCC guidelines, or guidelines previously published for each line.

Transfection and Cell Lysis: Transfection was carried out using Genejuice (Novagen) or Mirus LT1 (Mirus) for DNA plasmids as previously described (Garcia-Marcos et al., 2009; Ghosh et al., 2010). Lysates were prepared by resuspending cells in lysis buffer [20 mM HEPES, pH 7.2, 5 mM Mg-acetate, 125 mM K-acetate, 0.4% Triton X-100, 1 mM DTT, supplemented with sodium orthovanadate (500 μM), phosphatase (Sigma) and protease (Roche) inhibitor cocktails], after which they were passed through a 30G needle at 4°C, and cleared (10-14,000 g for 10 min) before being used in subsequent experiments.

***In cellulo* phosphorylation assays**: Cos7 cells expressing the indicated IMP probes in various assays were starved overnight at ~30 h after transfection, and subsequently treated with 0.2 mM Na_3VO_4 for 1 h prior to stimulation with growth factors or GPCR ligands. Cells were then washed with chilled PBS at 4˚C that was supplemented with 500 μM Na_3VO_4, lysed using ~400 μl of lysis buffer, and equal aliquots of lysates (~1-2 mg of total protein) were incubated for 4 hours at 4°C with either anti-GFP mouse monoclonal antibody (1 μg) (Lane et al., 2008) or control mouse IgG. Protein G Sepharose beads (GE Healthcare) were then added to the lysates and incubated at 4°C for additional 60 min. Beads were then washed 3 times using 1 ml of lysis buffer, and immune complexes were eluted by boiling in Laemmli's sample buffer. For steady state in vivo phosphorylation assays, IMP probes were co-transfected with Src or SHP1 constructs, and after 48 h of transfection cells were lysed and immunoprecipitated with anti-GFP mAb exactly as described for assays using ligand stimulation. In all assays tyrosine phosphorylation of IMP probes was detected by dual color immunoblotting with anti-pTyr mAb (BD Biosciences; Cat # 610000) and rabbit polyclonal anti-GFP using LiCOR Odyssey. Presence of yellow pixels on overlay of pTyr (green) and GFP (red) was interpreted as tyrosine phosphorylation of the IMP probe.

Scratch-wound healing assays: Sub-confluent (~85-90%) monolayers of HeLa cells were transiently transfected (exactly as outlined above) within 6-8 h after splitting with IMP constructs, grown to confluence over 24-30 h prior to scratch-wounding with the tip of a 200 μl pipette. The media was changed immediately afterwards to remove the scraped cells and avoid them from settling down. Wounds were imaged immediately after wounding at designated spots. The exact same coordinate was imaged again after 12 and 24 hours by light microscopy. Images were analyzed using ImageJ by outlining the borders of the wound at the beginning and end of the assay time points.

Förster Resonance Energy Transfer (FRET) studies: Intramolecular FRET was detected by sensitized emission using the three-cube method were performed as previously reported by Midde et al (Midde et al., 2015). All fluorescence microscopy assays were performed on single cells in mesoscopic regime to avoid inhomogeneities from samples as shown previously by Midde et al. (Borejdo et al., 2012; Midde et al., 2014). Briefly, cells were sparsely split into sterile 35 mm MatTek glass bottom dishes and transfected with 1 μg of various IMP constructs illustrated in **Fig. S3b**. An Olympus IX81 FV1000 inverted confocal laser scanning microscope was used for live cell FRET imaging (UCSD-Neuroscience core facility). The microscope is stabilized on a vibration proof platform, caged

in temperature controlled (37°C) and CO_2 (5%) supplemented chamber. A PlanApo 60x 1.40 N.A. oil immersed objective designed to minimize chromatic aberration and enhance resolution for 405-605 nm imaging was used. Olympus Fluoview inbuilt software was used for data acquisition. A 515 nm Argon-ion laser was used to excite EYFP and a 405 nm laser diode was used to excite ECFP as detailed by Claire Brown's group (Broussard et al., 2013). Spectral bleed-through coefficients were determined through FRET-imaging of donor-only and acceptor-only samples (i.e. cells expressing a single donor or acceptor FP). Enhanced CFP emission was collected from 425-500 nm and EYFP emission was collected through 535-600 nm and passed through a 50 nm confocal pinhole before being sent to a photomultiplier tube to reject out of plane focused light. Every field of view (FOV) is imaged sequentially through ECFPex/ECFPem, ECFPex/EYFPem and EYFPex/EYFPem (3 excitation and emission combinations) and saved as donor, FRET and acceptor image files through an inbuilt wizard. To obtain the FRET images and efficiency of energy transfer values a RiFRET plugin in Image J software was used (Roszik et al., 2009). Prior to FRET calculations, all images were first corrected for uneven illumination, registered, and background-subtracted. Manual and automatic registration of each individual channel in ImageJ was critical to correct for motion artifacts associated with live cell imaging. Controls were performed in which images were obtained in different orders. The order in which images were obtained had no effect. FRET images were obtained by pixel-by-pixel ratiometric intensity method and efficiency of transfer was calculated by the ratio of intensity in transfer channel to the quenched (corrected) intensity in the donor channel. The following corrections were applied to all FOVs imaged: For cross-talk correction, cells transfected with CFP or YFP alone were imaged under all three previously mentioned excitation and emission combinations. FRET efficiency was quantified from 3-4 Regions of Interests (ROI) per cell drawn exclusively along the P.M. Because expression of FRET probes may have a significant impact on FRET efficiency, cells that expressed similar amounts of probes, as determined by computing the fluorescence signal/intensity by a photon counting histogram were selectively chosen for FRET analyses. Furthermore, untransfected cells and a field of view with-out cells were imaged to correct for background, autofluorescence and light scattering. To avoid artifacts of photobleaching, Oxyfluor (www.oxyrase.com) was used to minimize the formation of reactive oxygen species.

Statistical Analyses: Data presented is representative of at-least 3 independent experiments and statistical significance was assessed by student t test, where p value < 0.05 at 95% was considered statistically significant. Statistical plots, including the Gaussian kernel density plot to the histogram were generated using GraphPad or OriginLab softwares.

SUPPLEMENTARY TABLES

Table S1: PhosphositePlus®(PSP) mining for Phosphoproteins observed in cancers [Related to Figure 1]. The PhosphoSitePlus(PSP) was mined for proteins expressed in all cancers. The search yielded 535 phosphosites in 324 proteins.

See Excel File – Table S1

Table S2: PhosphositePlus®(PSP) mining for Phosphoproteins observed in cancers that are not found in normal tissues [Related to Figure 1]. The PhosphoSitePlus(PSP) was mined for proteins expressed in all cancers and also excluded if expressed in normal tissue. The search yielded 113 phosphosites in 72 proteins.

See Excel File – Table S2

Table S3: PhosphositePlus®(PSP) mining revealed phosphoproteins observed in cancers that are also involved in cellular processes [Related to Figure 1]. The PhosphoSitePlus(PSP) was mined for proteins expressed in all cancers, excluded if expressed in normal tissue, and also involved in cellular processes. Such search yielded 149 phosphosites in 92 proteins.

See Excel File – Table S3

Table S4: PhosphositePlus®(PSP) mining for Phosphoproteins observed in cancers that are also binders and/or remodelers of actin [Related to Figure 1]. The PhosphoSitePlus(PSP) was mined for proteins expressed in all cancers, excluded if expressed in normal tissue, involved in cellular processes, and involved in regulating actin. The search yielded 63 phosphosites in 42 proteins.

See Excel File – Table S4

Table S5: PhosphositePlus®(PSP) mining for Phosphoproteins observed in cancers that are actin-binding adaptors/scaffolds and are involved in cell migration [Related to Figure 1]. The PhosphoSitePlus(PSP) was mined for proteins expressed in all cancers, excluded if expressed in normal tissue, involved in cellular processes, involved in regulating actin and also involved in migration. The search yielded 34 phosphosites in 16 proteins.

See Excel File – Table S5

SUPPLEMENTARY FIGURES AND LEGENDS

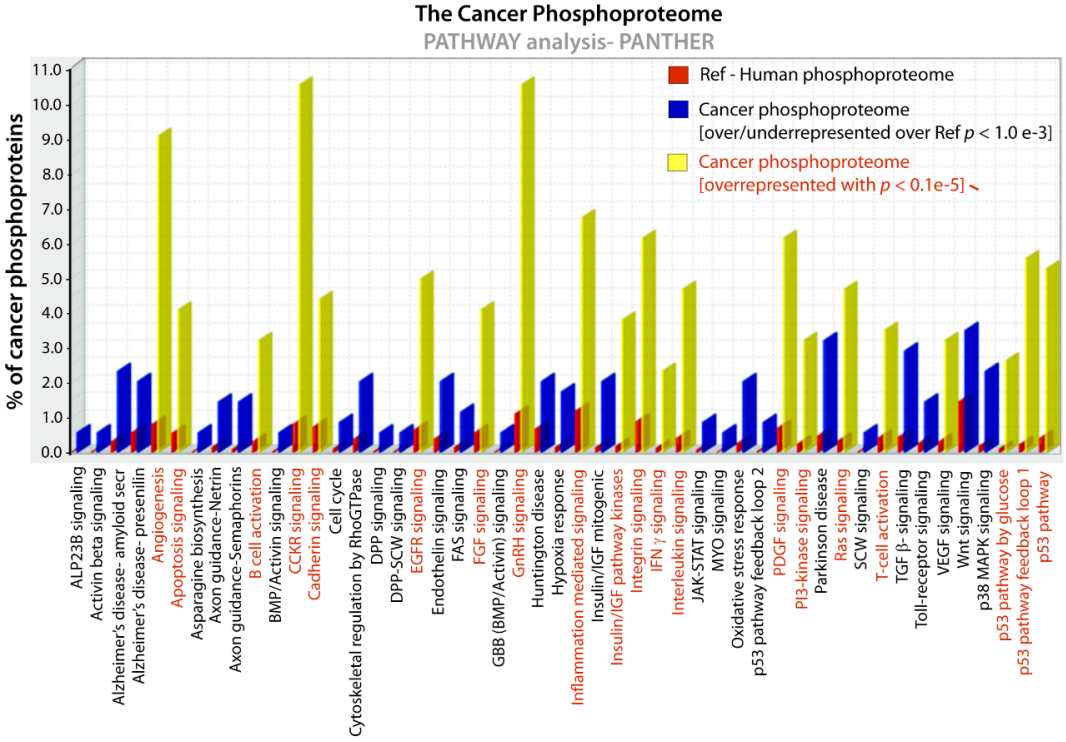

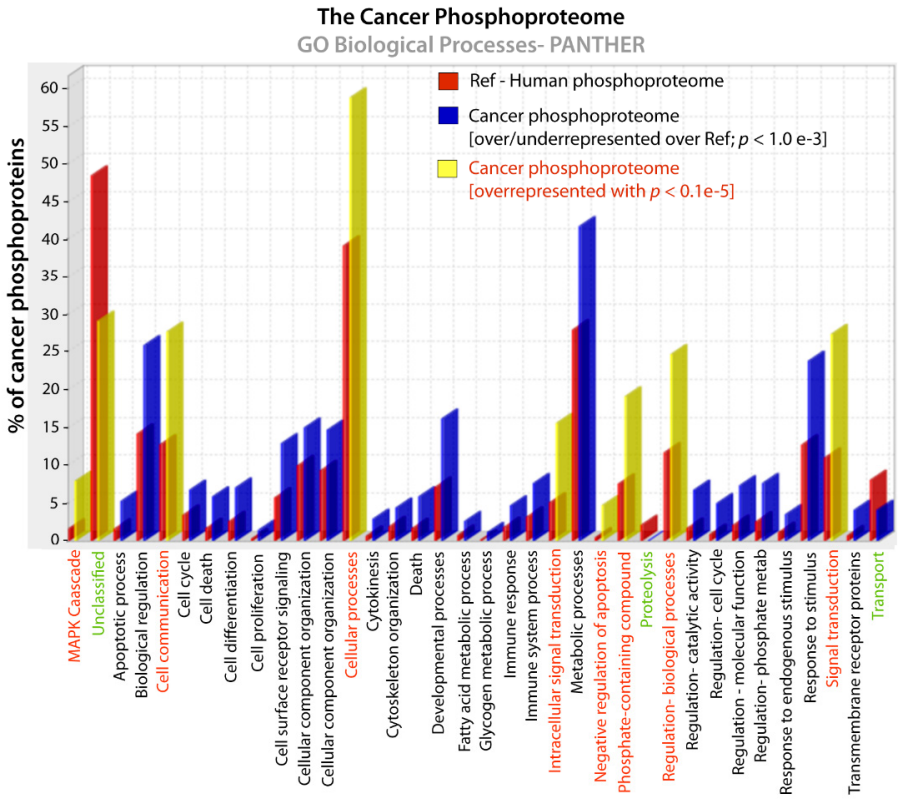

Figure S1. Mining the PhosphositePlus® (PSP) database for pan-cancer phosphoproteome [Related to Figure 1]. A list of 324 proteins whose phosphosites are observed in cancers (see **Table S1**) were subjected to an enrichment analysis using analysis tools from the PANTHER Classification System (Mi et al., 2013). Pathways (a) and GO-biological processes (b) enriched among these 324 proteins compared to the entire human phosphoproteome as reference are displayed. % of protein in the category is calculated for each list (the human phosphoproteome reference list and the pan- cancer phosphoproteome list) as: (# proteins for the category/ # proteins in the list) X 100. Underrepresented pathways are highlighted in green.

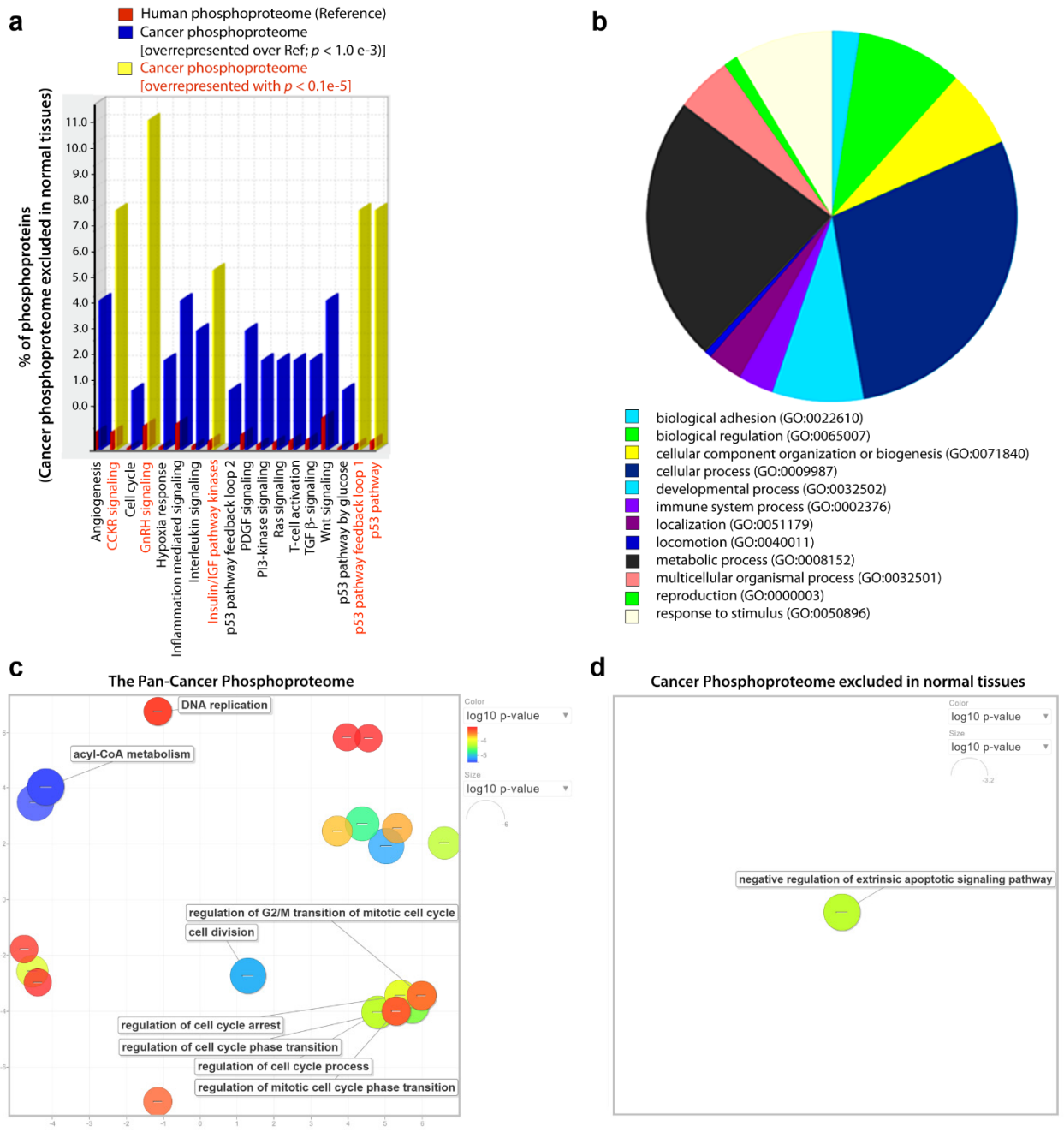

Figure S2. Mining the PhosphositePlus (PSP) database and visualizing GO enrichment in the cancer-specific phosphoproteome [Related to Figure 1]. (a-b) A list of 72 phosphoproteins from the PSP database that fit the criteria for being found in cancers but excluded in normal tissues (see **Table S2**) were subjected to an enrichment analysis using analysis tools from the PANTHER Classification System (Mi et al., 2013). Pathways (a) and GO biological processes (b) enriched among these 72 proteins compared to the entire human phosphoproteome as reference are displayed. (c-d) The list of phosphoproteins observed in cancers (**Table S1**) and the list of phosphoproteins observed in cancers but excluded in normal tissues (**Table S2**) were submitted to the Reduce + Visualize Gene Ontology (REVIGO (Supek et al., 2011)) analysis tool and GO terms were visualized in a semantic similarity-based scatterplots on left and right, respectively. GO-biological process enriched in the pan-cancer phosphoproteome (left) is notable for regulators of cell cycle, DNA replication and multiple metabolic pathways. By contrast, negative regulation of apoptotic signaling pathway is the only GO-biological process that is enriched in the cancer-specific phosphoproteome (i.e., phosphoproteins observed in cancers, not in normal tissues). The colors do not reflect pathway direction but rather the degree of statistical significance. Red circles indicate regulated pathways that are different to a highly significant degree; green and blue also indicate significant difference, but to a lesser degree. The color intensity represents the negative log10 *p* value for each of the statistically enriched pathways shown on the scatterplot.

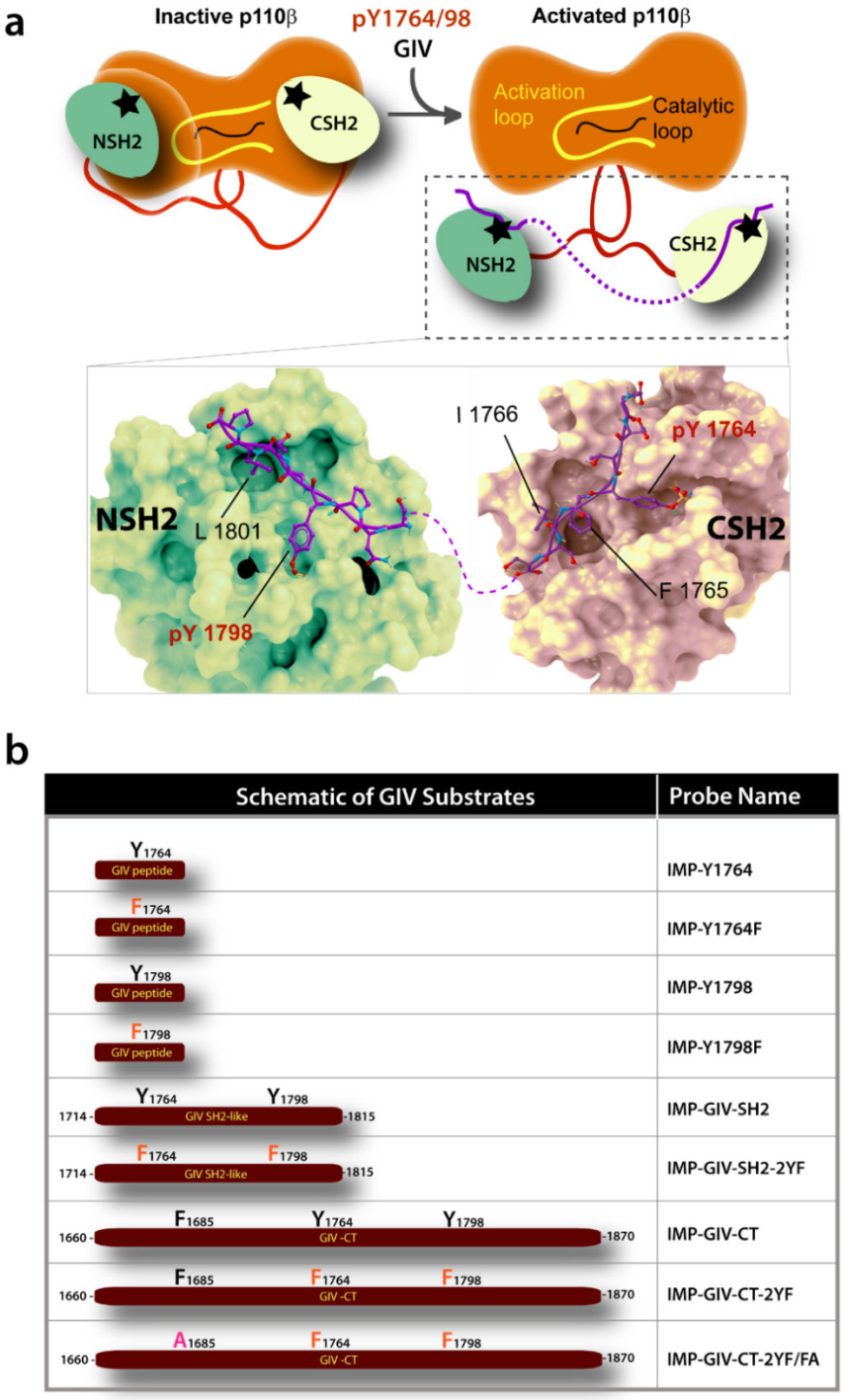

Figure S3. **Rationale for the modular design of IMP probes [Relevant to Figure 1].** (a) Previously validated (Lin et al., 2011) structural basis for activation of PI3K by GIV is displayed. Phosphotyrosines 1764 and 1798 on GIV directly bind p85α (SH2-domains) and activate Class 1 PI3Ks. (b) Various GIV-derived IMPs generated and tested in this work; they either contain the two short stretches of sequence flanking either tyrosine 1764 or 1798 alone, or together (entire SH2 module) or in combination with GIV's GEF module (entire C-Term). Non-phosphorylatable phenylalanine mutants were generated in each case to serve as negative controls. These GIV substrates were inserted within the IMP probe shown in *Fig 1c*.

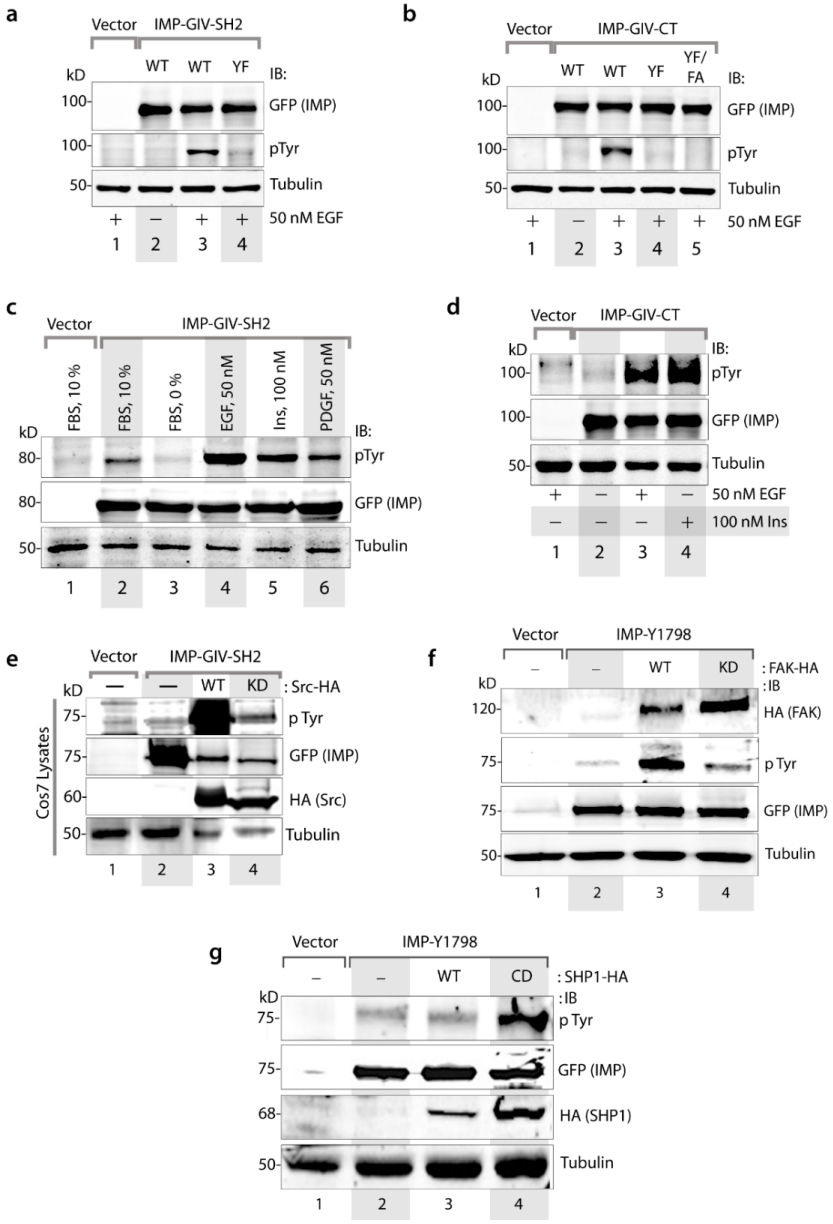

Figure S4. GIV-derived IMP probes are reversibly tyrosine phosphorylated in cells [Related to Figure 1]. (a) Immunoblots showing the phosphorylation status of WT IMP-GIV-SH2 and its corresponding YF mutant after EGF stimulation. Only WT IMP peptides are phosphorylated but not its corresponding YF mutants. (b) Immunoblots showing the phosphorylation status of WT IMP-GIV-CT and their corresponding YF and YF/FA mutants after EGF stimulation. Only WT IMP-GIV-CT probe gets phosphorylated but not its corresponding YF mutant (c) Serum-starved Cos7 cells expressing WT IMP-GIV-SH2 were stimulated with various growth factors prior to lysis. Lysates were immunoprecipitated with anti-GFP mAb and tyrosine phosphorylation of IMP-GIV-SH2 probe was analyzed by immunoblotting (IB). Phosphorylation of the peptide was observed in fed state (10% FBS) or when stimulated with EGF or Insulin or PDGF but not in overnight starved conditions. (d) Serum-starved Cos7 cells expressing WT IMP-GIV-CT were stimulated with EGF or Insulin prior to lysis. Lysates were immunoprecipitated with anti-GFP mAb and tyrosine phosphorylation of IMP was analyzed by immunoblotting (IB). Phosphorylation of the IMP-GIV-CT-WT probe was only observed in cells when stimulated with either EGF or insulin but not in starved cells. (e) Lysates of Cos7 cells co-expressing IMP-GIV-SH2 and wild-type (WT) or kinase-dead (KD) Src-HA were immunoprecipitated and analyzed for tyrosine phosphorylation of IMP as in d. Phosphorylation of the IMP-GIV-SH2 probe was only observed in cells co-transfected with Src-HA-WT but not in cells transfected with kinase dead Src-HA-KD cells. (f) Lysates of Cos7 cells expressing IMP-GIVY1798 and wild-type (WT) or Kinase Dead (KD) FAK-HA were immunoprecipitated and analyzed for tyrosine phosphorylation of IMP as in d. Phosphorylation of the IMP-GIV-SH2 probe was only detected in cells expressing WT-FAK-HA but in kinase dead FAK-HA expressing cells. (g) Lysates of Cos7 cells expressing IMP-GIV&1798 and wild-type (WT) or catalytically dead (CD) SHP1-HA were immunoprecipitated and analyzed for tyrosine phosphorylation of IMP as in d. Phosphorylation of the IMP-GIVY1798 probe was only detected in cells expressing SHP1-HA-CD but in SHP1-HA-WT expressing cells.

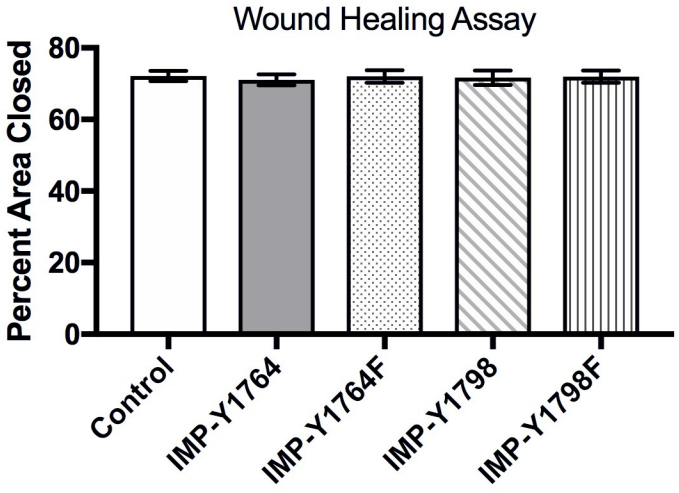

Figure S5. Transient overexpression of IMP 1764 and IMP1798 does not alter 2D cell migration in scratch-wound assays [Related to Figure 1]. Sub-confluent (~85-90%) monolayers of HeLa cells transiently transfected with the indicated IMP constructs were grown to confluence over 30 h prior to scratch-wounding. Wounds were imaged immediately after wounding and again, after 12 and 24 hours by light microscopy. Bar graphs display the % wound closure, as determined by tracing the exposed wound area at the beginning and at 24 h using ImageJ was measured. Error bars represent ±SEM; n = 4-5 wounds per cell line, per experiment, from 3 independent biological repeat experiments.

a

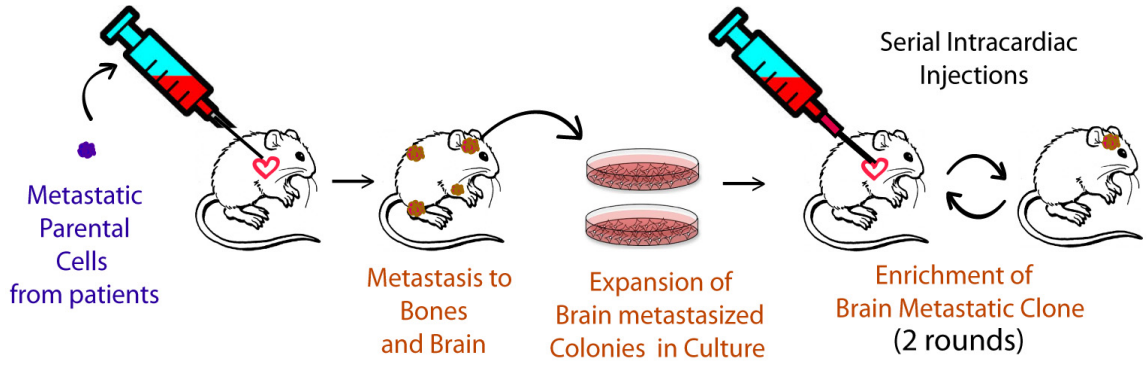

b

Paired Cell Lines	Type of Cancer	Source of Parental Cells	Known Genetic Mutations	Ref PMID (Source Lab)
MDAMB231 (Parental and Brain Metastatic Clone)	Human Breast Adenocarcinoma	Metastatic Pleural Effusion	*KRAS* G13D, *BRAF*G464V PMID: 17314276	24581498 (J. Massague)
PC-9 (Parental and Brain Metastatic Clone)	Human Lung Adenocarcinoma	Metastatic clone from lymph node	KRAS (G12C) PMID: 8806092	19576624 24581498 (J. Massague)
H2030 (Parental and Brain Metastatic Clone)	Human Lung Adenocarcinoma	Metastatic clone from lymph node	$EGFR^{\Delta exon19}$ PMID: 15761868, PMID: 1847845	19576624 24581498 (J. Massague)
21T (16N, NT, MT2)	Human Breast Infiltrating and intraductal mammary carcinoma (ER-/PR-; Node +) PMID: 1977518	16N = Normal, Contralateral Breast NT = Primary Tumor MT2 = Metastatic Pleural Effusion	In NT and MT2 - p53 (frameshift mutation, loss of function (PMID: 7923592)	20198662 20458274 17545609 (A. Pardee)

Figure S6. Sources of various paired cancer cell lines used in the study [Related to Figure 3]. (a) Schematic representing the technique that was employed by Massague et al (Nguyen et al., 2009) to generate paired primary and Brain metastatic clones. Briefly, 10^5 of metastatic lung or breast cancer cells isolated from lymphatic duct or pleural effusions of cancer patients were injected into arterial circulation of nude mice. Subsequently, tumor cells were isolated from lesions formed at secondary site i. e. brain or bone, followed by expansion of the cells and reinjection of the cells into mice circulation for two more rounds to select for highly metastatic clones. (b) List of paired (parental and brain mets) lung and breast cancer cell lines with variable metastatic proclivity used in the study, their varying genetic background, and known mutations and the sources of cells.

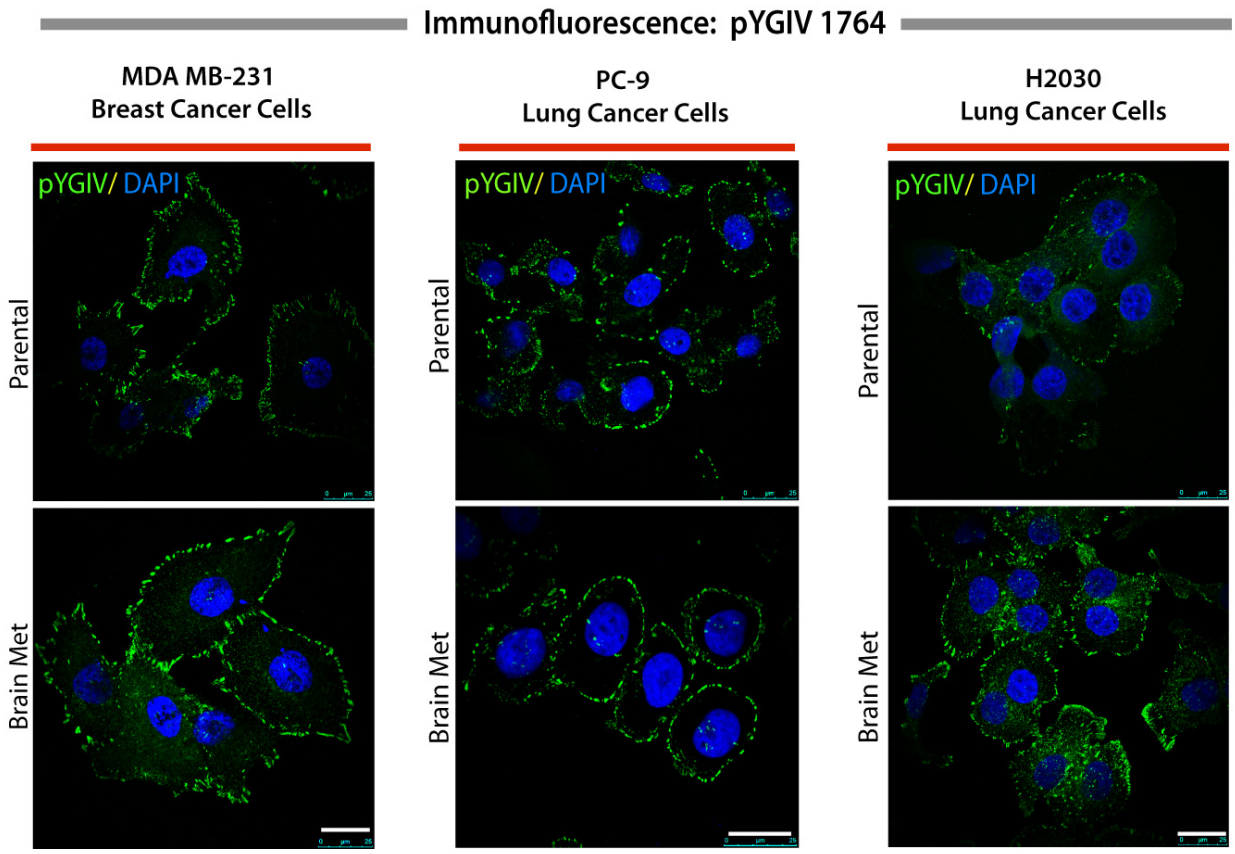

Figure S7. Tyrosine phosphorylation of GIV is indistinguishable among paired primary and BrM breast and lung cancer cells by Immunofluorescence [Related to Figure 3]. PC-9, H2030, MDA-MB-231 primary and their BrM counterparts were fixed, stained for tyrosine phosphorylated GIV (pYGIV; red) and DAPI (nucleus; blue) and analyzed by confocal microscopy. Representative images of cells are shown. Although cell-to-cell heterogeneity in intensity of staining was encountered, no discernable differences in patterns of staining was observed between the parental and BrM clones. Bar = 10 μm.

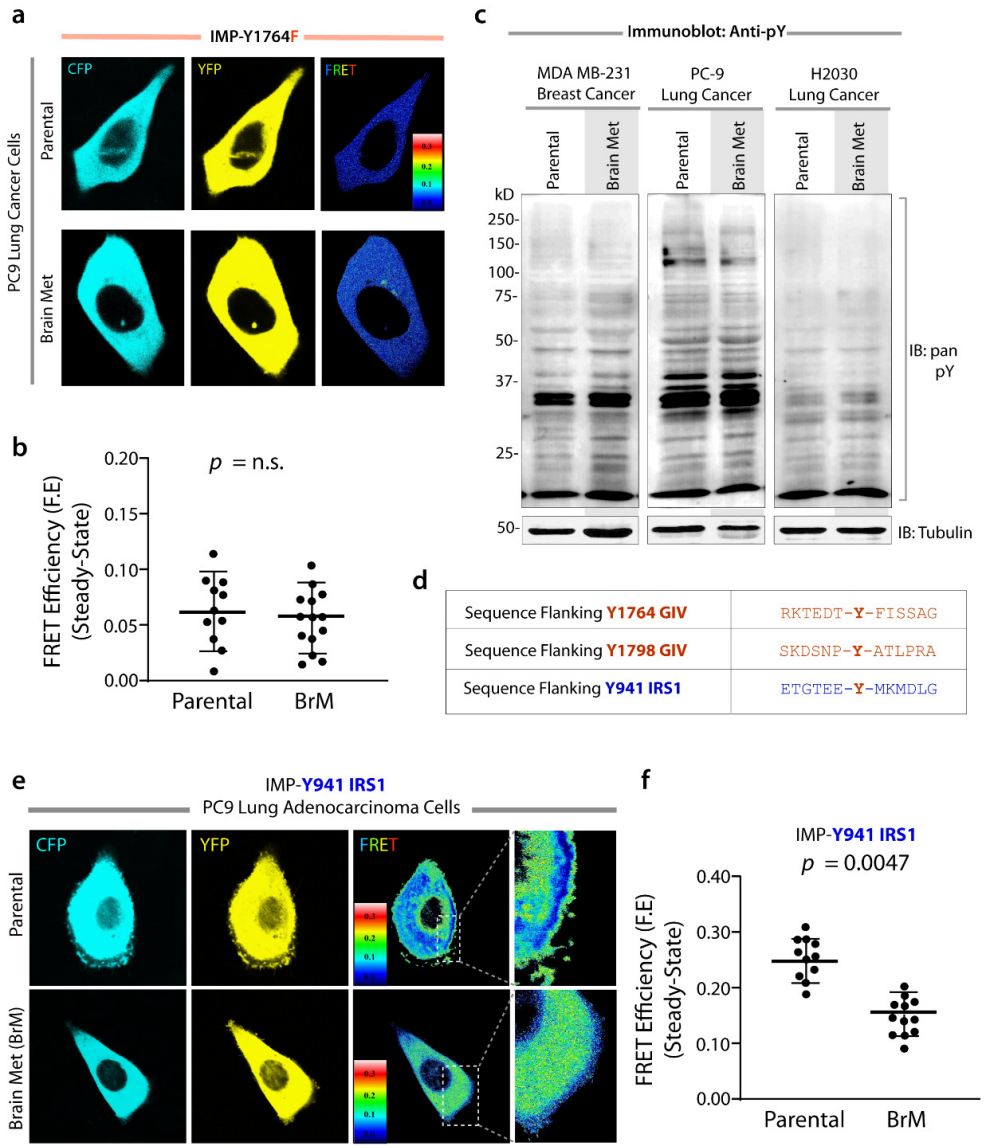

Figure S8. Control experiments that show the specificity of IMP probes to detect meaningful, context-dependent signals [Related to Figure 3]. (a-b) Representative steady state FRET images of PC-9 parental and BrM cells expressing IMP-Y1764F mutant probe. IMP Y1764F mutant peptide shows no differential FRET signal when expressed in paired cancer cell lines; very little FRET was observed in both the parental and BrM PC-9 cell groups at steady state in 10% serum, indicating that tyrosine phosphorylation of the IMP probe is essential for the differential FRET observed in these cells using the WT probe *2e*. (b) Scatter plots display the FRET efficiency at the PM in *a*. Results are expressed as mean ± S.D. (c) Whole cell lysates from paired PC-9, H2030 and MDA-MB-231 cells were immunoblotted with total phosphorylated tyrosine antibody. Full-length phosphotyrosine immunoblot shows no discernable differences in either global tyrosine phosphorylation or tyrosine phosphorylation at any given molecular weight between the parental and the BrM clones. Results indicate that the differences in FRET in these paired cells observed using the IMP-Y1764 probe in *2d-f* does not merely reflect global differences in tyrosine phosphorylation. (d-f) Replacement of the GIV substrate sequence with a sequence derived from IRS1 abolishes the ability of IMP probes to distinguish cancer cells with high from low metastatic potential. (d) Schematic showing the substrate sequence of GIV used in IMP-Y1764 and IMP-Y1798 probes, and the sequence of IRS1 that was used to substitute the residues flanking the Y substrate. Previous work has shown that this site is phosphorylated by multiple growth factors (EGF, PDGF and Insulin) (Sato et al., 2002) and is a binding site for p85α(PI3K) (Yonezawa et al., 1992) and induces FRET when used in similar probe design as IMPs (Sato et al., 2002). (e) Parental and brain metastatic (BrM) clones of PC-9 lung cancer cells expressing IMP-Y941 IRS were analyzed for steady-state FRET by confocal live-cell imaging. Representative CFP, YFP and FRET images are shown. Boxed area on the left is magnified on the right. FRET is frequently observed at the PM in parental, but not in BrM clones. (f) Scatter plots display the FRET efficiency at the PM in e. Results are expressed as mean ± S.D.

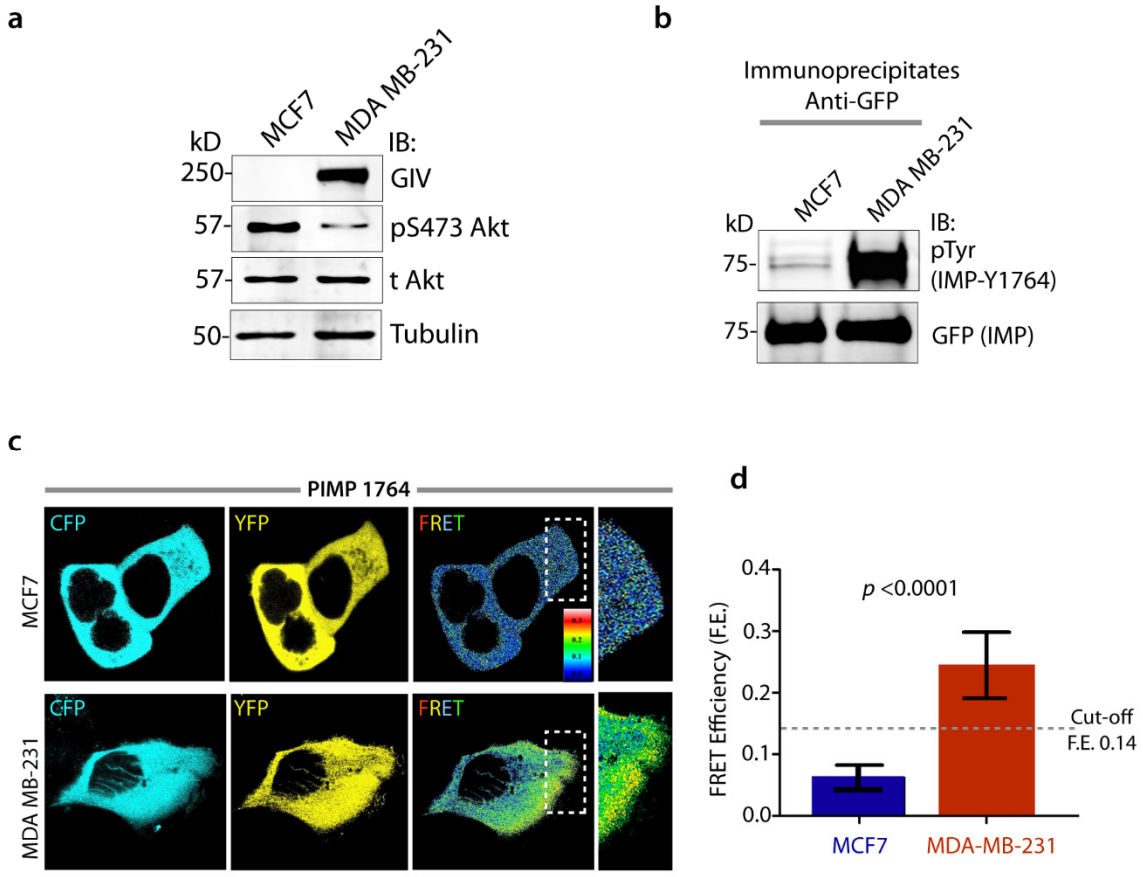

Figure S9. IMP sensors can distinguish between MCF7 and MDA-MB-231 cells, two breast cancer cell lines with contrasting metastatic proclivities [Related to Figure 3]. (a) Whole cell lysates of MCF7 and MDA-MB-231 cells were analyzed for GIV, phospho(p)Akt, total(t)Akt and tubulin by immunoblotting (IB). (b) Immunoprecipitation was carried out from lysates of MCF7 and MDA-MB-231 cells expressing IMP-Y1764 with anti-GFP mAb and analyzed for tyrosine phosphorylation of IMP by immunoblotting (IB). (c) MCF7 and MDA-MB-231 cells expressing IMP-Y1764 were analyzed for steady-state FRET by confocal live-cell imaging. Representative CFP, YFP and FRET images are shown. Boxed area on the left is magnified on the right. (d) Bar graphs display the FRET efficiency (F.E) in c. The cut-off F.E of 0.14 (based on the cumulative histograms in *Fig 3g*) denotes that MCF7 cells with low F.E and MDA-MB-231 cells with high F.E have low and high metastatic potentials, respectively. Results are expressed as mean ± S.D.

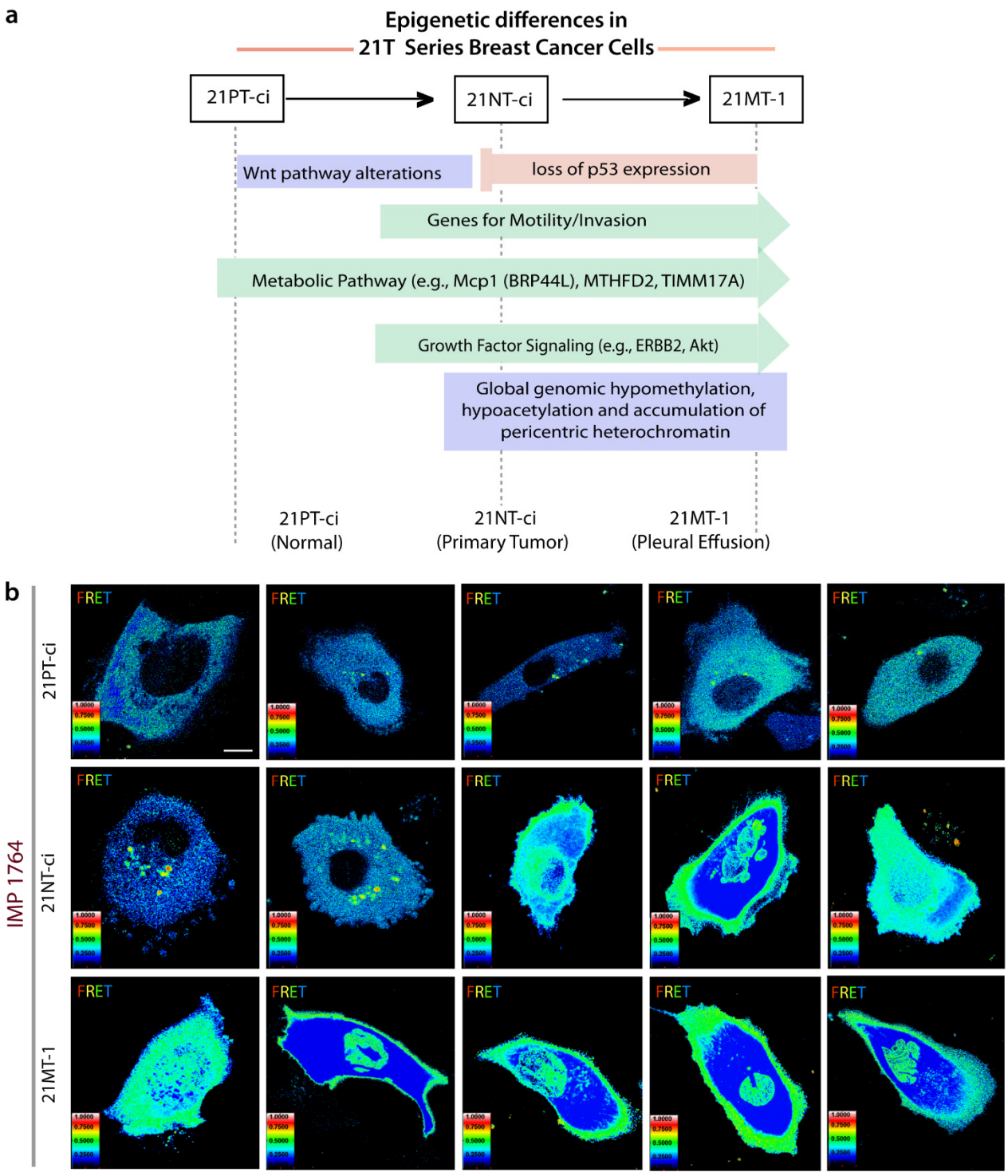

Figure S10. IMPY1764 sensor retains its ability to detect metastatic proclivity despite the evolving genetic and epigenetic shifts in tumor cells during the course of metastatic progression [Related to Figure 3]. (a) Schematic summarizing the characteristics of the 21T series of breast cancer cells. These isogenic cells were derived from the same patient (#21) during breast cancer progression (Band et al., 1990) (*Fig 3h*). The array of evolving epigenetic (Liu et al., 1994; Santos et al., 2014; Souter et al., 2010), proteomic (Xu et al., 2010) and signaling (MacMillan et al., 2014; Qiao et al., 2007) programs during progressive acquisition of metastatic potential are summarized. *(b)* 21T cells expressing IMP-Y1764 were analyzed for steady-state FRET by confocal live-cell imaging. Representative FRET images are shown as a montage of single-cells images. Quantifications are displayed as scatter plots in *Fig 3i*.

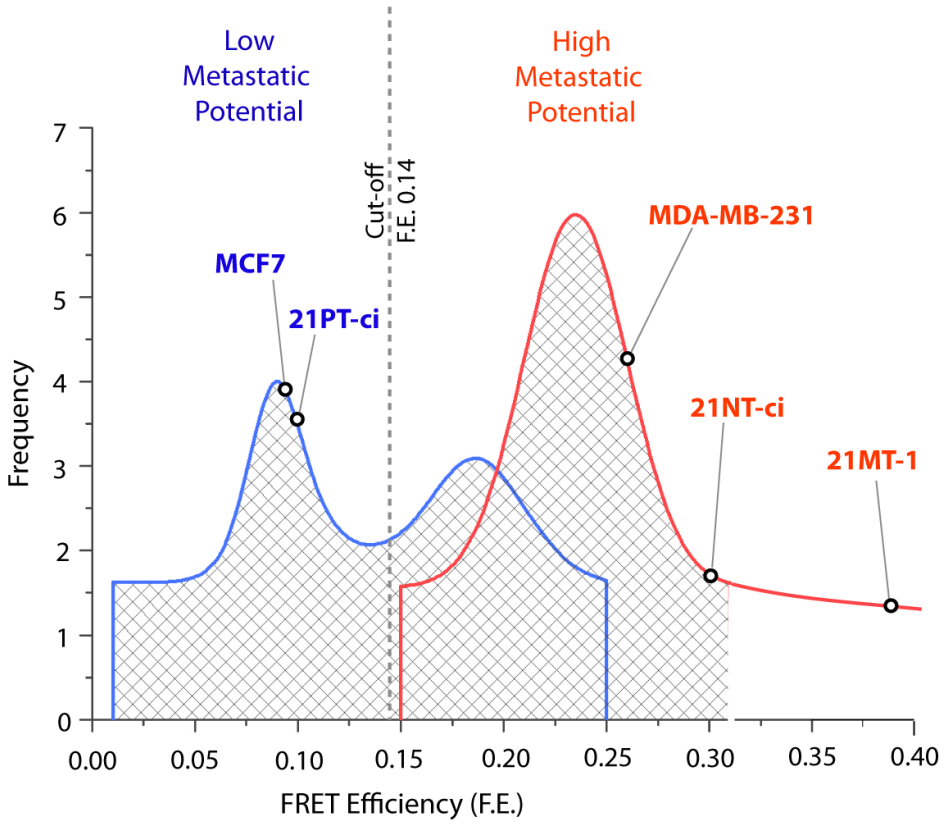

Figure S11. Gaussian Fits of FRET histograms [Related to Figure 3]. Gaussian fits of the cumulative histogram in *Fig 3g* is displayed here with the position of various cell lines (mean FRET) studied in this work indicated on the gaussian curve.

a

Paired Cell Lines	Type of Cancer	Pathways Upregulated During Drug Resistance	Known Genetic Abnormalities	Ref PMID (Source Lab)
Hs578T (Docetaxel sensitive vs resistant)	Human Breast	**Multiple pathways, including mTOR and TNF-dependent NF-κB survival pathways.** (PMID: 15718313; 12907009)	ER -ve; Hypotriploid human cell line with a modal chromosome number of 59 (ATCC.org) (PMID: 864756)	ATCC
HCC827 (Erlotinib sensitive vs resistant)	Human Lung Adenocarcinoma	**PI3K** (PMID: 21220474) **Non-RTK Signaling (Src/FAK)** (PMID:25193862; 19804422) **Gowth Factor RTK Signaling (cMet, VEGF, IGFR)** (PMID:24828661; 22133747; 21062933; 19921194; 19447865) **STAT3** (PMID: 23894143) **mTOR** (PMID: 23690929)	EGFR tyrosine kinase domain (E746 - A750 deletion) (ATCC.org)	Frank Furnari (UCSD)
HCC827 (Lapatinib sensitive vs resistant)	Human Lung Adenocarcinoma	--	EGFR tyrosine kinase domain (E746 - A750 deletion) (ATCC.org)	David Cheresh (PMID: 24747441)

b

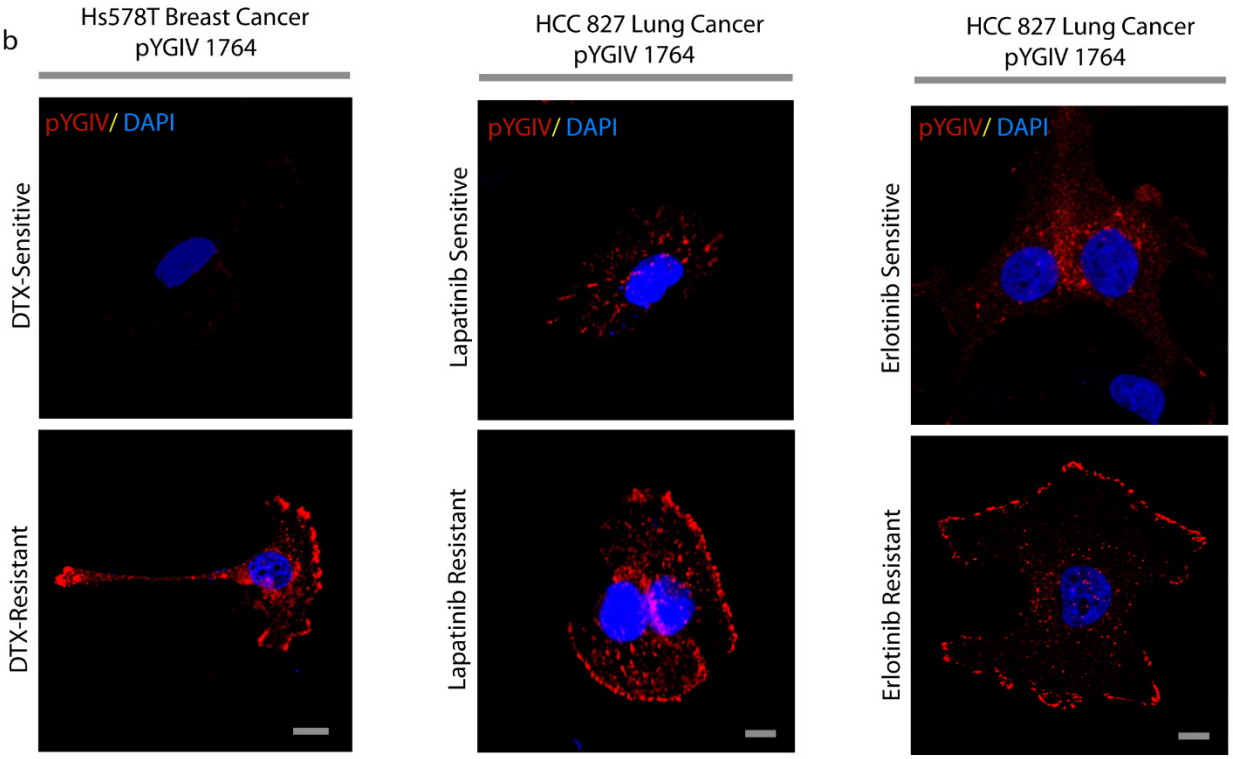

Figure S12. Tyrosine phosphorylation of GIV at the PM is enhanced during drug resistance [Related to Figure 4]. (a) Table lists the paired (sensitive vs resistant) breast (Hs578T) and lung (HCC827) cancer cells used in this study, the underlying pathways implicated in the development of drug resistance, the genetic background and the source of cells. (b) Docetaxel (DTX)-sensitive and resistant pairs of Hs578T, and Lapatinib/Erlotinib sensitive and resistant pairs of HCC827 cells were fixed, stained for tyrosine phosphorylated GIV (pYGIV; red) and DAPI (nucleus; blue) and analyzed by confocal microscopy. Representative images of cells are shown. Bar = 10 μm.

SUPPLEMENTARY MOVIE CAPTIONS

SM1. Dynamic changes in FRET at the PM upon EGF stimulation of Cos7 cells expressing the IMP-pY1764 probe [Related to Figure 2]. Movie shows ligand-dependent signaling via the GIV-PI3K axis as visualized through FRET imaging in living Cos7 cells expressing the wild type IMP-Y1764 sensor.

SM2. Loss of dynamic changes in FRET upon EGF stimulation [Related to Figure 2]. Movie shows loss of FRET upon EGF stim in of Cos7 cells expressing the non-phosphorylatable IMP-pY1764F mutant probe, indicating that phosphorylation and phosphorylation-induced intramolecular rearrangement of the probe is required for the observed changes in FRET in SM1.

SM3. Dynamic changes in FRET at the PM upon EGF stimulation of Cos7 cells expressing the IMP-pY1798 probe [Related to Figure 2]. Movie shows ligand-dependent signaling via the GIV-PI3K axis as visualized through FRET imaging in living Cos7 cells expressing the wild type IMP-Y1798 sensor.

SM4. Loss of dynamic changes in FRET upon EGF stimulation of Cos7 cells expressing the non-phosphorylatable IMP-pY1798F mutant probe [Related to Figure 2]. This movie indicates that phosphorylation and phosphorylation-induced intramolecular rearrangement of the probe is required for the observed changes in FRET in SM3.

SM5. Dynamic changes in FRET at the PM upon LPA stimulation of Cos7 cells expressing the IMP-pY1764 probe [Related to Figure 2]. Movie shows ligand-dependent signaling via the GIV-PI3K axis as visualized through FRET imaging in living Cos7 cells expressing the wild type IMP-Y1764 sensor.

SM6. Loss of dynamic changes in FRET upon LPA stimulation of Cos7 cells expressing the non-phosphorylatable IMP-pY1764F mutant probe [Related to Figure 2]. This movie indicates that phosphorylation and phosphorylation-induced intramolecular rearrangement of the probe is required for the observed dynamic changes in FRET in SM5.

SUPPLEMENTARY BIBLIOGRAPHY

Band, V., Zajchowski, D., Swisshelm, K., Trask, D., Kulesa, V., Cohen, C., Connolly, J., and Sager, R. (1990). Tumor progression in four mammary epithelial cell lines derived from the same patient. Cancer research *50*, 7351-7357.

Borejdo, J., Rich, R., and Midde, K. (2012). Mesoscopic analysis of motion and conformation of cross-bridges. Biophys Rev *4*, 299-311.

Broussard, J.A., Rappaz, B., Webb, D.J., and Brown, C.M. (2013). Fluorescence resonance energy transfer microscopy as demonstrated by measuring the activation of the serine/threonine kinase Akt. Nature protocols *8*, 265-281.

Brown, I., Shalli, K., McDonald, S.L., Moir, S.E., Hutcheon, A.W., Heys, S.D., and Schofield, A.C. (2004). Reduced expression of p27 is a novel mechanism of docetaxel resistance in breast cancer cells. Breast cancer research : BCR *6*, R601-607.

Garcia-Marcos, M., Ghosh, P., and Farquhar, M.G. (2009). GIV is a nonreceptor GEF for G alpha i with a unique motif that regulates Akt signaling. Proceedings of the National Academy of Sciences of the United States of America *106*, 3178-3183.

Garcia-Marcos, M., Jung, B.H., Ear, J., Cabrera, B., Carethers, J.M., and Ghosh, P. (2011). Expression of GIV/Girdin, a metastasis-related protein, predicts patient survival in colon cancer. FASEB journal : official publication of the Federation of American Societies for Experimental Biology *25*, 590-599.

Ghosh, P., Beas, A.O., Bornheimer, S.J., Garcia-Marcos, M., Forry, E.P., Johannson, C., Ear, J., Jung, B.H., Cabrera, B., Carethers, J.M*., et al.* (2010). A Gi-GIV Molecular Complex Binds Epidermal Growth Factor Receptor and Determines whether Cells Migrate or Proliferate. Molecular biology of the cell.

Griesbeck, O., Baird, G.S., Campbell, R.E., Zacharias, D.A., and Tsien, R.Y. (2001). Reducing the environmental sensitivity of yellow fluorescent protein. Mechanism and applications. The Journal of biological chemistry *276*, 29188-29194.

Jost, C.A., Reither, G., Hoffmann, C., and Schultz, C. (2008). Contribution of fluorophores to protein kinase C FRET probe performance. Chembiochem *9*, 1379-1384.

Kotera, I., Iwasaki, T., Imamura, H., Noji, H., and Nagai, T. (2010). Reversible dimerization of Aequorea victoria fluorescent proteins increases the dynamic range of FRET-based indicators. ACS Chem Biol *5*, 215-222.

Lane, J.R., Powney, B., Wise, A., Rees, S., and Milligan, G. (2008). G protein coupling and ligand selectivity of the D2L and D3 dopamine receptors. The Journal of pharmacology and experimental therapeutics *325*, 319-330.

Li, C., Wen, A., Shen, B., Lu, J., Huang, Y., and Chang, Y. (2011). FastCloning: a highly simplified, purification-free, sequence- and ligation-independent PCR cloning method. BMC biotechnology *11*, 92.

Lin, C., Ear, J., Pavlova, Y., Mittal, Y., Kufareva, I., Ghassemian, M., Abagyan, R., Garcia-Marcos, M., and Ghosh, P. (2011). Tyrosine phosphorylation of the Galpha-interacting protein GIV promotes activation of phosphoinositide 3-kinase during cell migration. Science signaling *4*, ra64.

Liu, X.L., Band, H., Gao, Q., Wazer, D.E., Chu, Q., and Band, V. (1994). Tumor cell-specific loss of p53 protein in a unique in vitro model of human breast tumor progression. Carcinogenesis *15*, 1969-1973.

Lopez-Sanchez, I., Dunkel, Y., Roh, Y.S., Mittal, Y., De Minicis, S., Muranyi, A., Singh, S., Shanmugam, K., Aroonsakool, N., Murray, F*., et al.* (2014). GIV/Girdin is a central hub for profibrogenic signalling networks during liver fibrosis. Nature communications *5*, 4451.

MacMillan, C.D., Leong, H.S., Dales, D.W., Robertson, A.E., Lewis, J.D., Chambers, A.F., and Tuck, A.B. (2014). Stage of breast cancer progression influences cellular response to activation of the WNT/planar cell polarity pathway. Scientific reports *4*, 6315.

Mi, H., Muruganujan, A., Casagrande, J.T., and Thomas, P.D. (2013). Large-scale gene function analysis with the PANTHER classification system. Nature protocols *8*, 1551-1566.

Midde, K., Rich, R., Saxena, A., Gryczynski, I., Borejdo, J., and Das, H.K. (2014). Membrane topology of human presenilin-1 in SK-N-SH cells determined by fluorescence correlation spectroscopy and fluorescent energy transfer. Cell biochemistry and biophysics *70*, 923-932.

Midde, K.K., Aznar, N., Laederich, M.B., Ma, G.S., Kunkel, M.T., Newton, A.C., and Ghosh, P. (2015). Multimodular biosensors reveal a novel platform for activation of G proteins by growth factor receptors. Proceedings of the National Academy of Sciences of the United States of America *112*, E937-946.

Mittal, Y., Pavlova, Y., Garcia-Marcos, M., and Ghosh, P. (2011). Src homology domain 2-containing protein-tyrosine phosphatase-1 (SHP-1) binds and dephosphorylates G(alpha)-interacting, vesicle-associated protein (GIV)/Girdin and attenuates the GIV-phosphatidylinositol 3-kinase (PI3K)-Akt signaling pathway. The Journal of biological chemistry *286*, 32404-32415.

Nguyen, D.X., Chiang, A.C., Zhang, X.H., Kim, J.Y., Kris, M.G., Ladanyi, M., Gerald, W.L., and Massague, J. (2009). WNT/TCF signaling through LEF1 and HOXB9 mediates lung adenocarcinoma metastasis. Cell *138*, 51-62.

Qiao, M., Iglehart, J.D., and Pardee, A.B. (2007). Metastatic potential of 21T human breast cancer cells depends on Akt/protein kinase B activation. Cancer research *67*, 5293-5299.

Roszik, J., Lisboa, D., Szollosi, J., and Vereb, G. (2009). Evaluation of intensity-based ratiometric FRET in image cytometry--approaches and a software solution. Cytometry Part A : the journal of the International Society for Analytical Cytology *75*, 761-767.

Santos, G.C., Jr., da Silva, A.P., Feldman, L., Ventura, G.M., Vassetzky, Y., and de Moura Gallo, C.V. (2014). Epigenetic modifications, chromatin distribution and TP53 transcription in a model of breast cancer progression. Journal of cellular biochemistry.

Sato, M., Ozawa, T., Inukai, K., Asano, T., and Umezawa, Y. (2002). Fluorescent indicators for imaging protein phosphorylation in single living cells. Nature biotechnology *20*, 287-294.

Souter, L.H., Andrews, J.D., Zhang, G., Cook, A.C., Postenka, C.O., Al-Katib, W., Leong, H.S., Rodenhiser, D.I., Chambers, A.F., and Tuck, A.B. (2010). Human 21T breast epithelial cell lines mimic breast cancer progression in vivo and in vitro and show stage-specific gene expression patterns. Laboratory investigation; a journal of technical methods and pathology *90*, 1247-1258.

Supek, F., Bosnjak, M., Skunca, N., and Smuc, T. (2011). REVIGO summarizes and visualizes long lists of gene ontology terms. PLoS One *6*, e21800.

Ullman, K.S., Powers, M.A., and Forbes, D.J. (1997). Nuclear export receptors: from importin to exportin. Cell *90*, 967-970.

Valiente, M., Obenauf, A.C., Jin, X., Chen, Q., Zhang, X.H., Lee, D.J., Chaft, J.E., Kris, M.G., Huse, J.T., Brogi, E.*, et al.* (2014). Serpins promote cancer cell survival and vascular co-option in brain metastasis. Cell *156*, 1002-1016.

Xu, X., Qiao, M., Zhang, Y., Jiang, Y., Wei, P., Yao, J., Gu, B., Wang, Y., Lu, J., Wang, Z.*, et al.* (2010). Quantitative proteomics study of breast cancer cell lines isolated from a single patient: discovery of TIMM17A as a marker for breast cancer. Proteomics *10*, 1374-1390.

Yonezawa, K., Ueda, H., Hara, K., Nishida, K., Ando, A., Chavanieu, A., Matsuba, H., Shii, K., Yokono, K., Fukui, Y.*, et al.* (1992). Insulin-dependent formation of a complex containing an 85-kDa subunit of phosphatidylinositol 3-kinase and tyrosine-phosphorylated insulin receptor substrate 1. The Journal of biological chemistry *267*, 25958-25965.